The investigation of HCO_3^- secretion in pancreatic ductal organoid cultures

Réka Molnár

Ph.D. Thesis

Supervisor: József Maléth, M.D., Ph.D

Theoretical Medicine Doctoral School

First Department of Medicine

University of Szeged

Szeged, Hungary

2020

LIST OF FULL PAPERS RELATED TO THE THESIS

Articles closely related to the subject of the thesis and cited in the thesis:

I. **Molnár R**, Madácsy T, Varga Á, Németh M, Katona X, Görög M, Molnár B, Fanczal J, Rakonczay Z Jr, Hegyi P, Pallagi P, Maléth J., Mouse pancreatic ductal organoid culture as a relevant model to study exocrine pancreatic ion secretion.
Lab Invest. 2020 Jan; doi: 10.1038/s41374-019-0300-3
[IF_{2018}: 3.684]

II. Fanczal J, Pallagi P, Görög M, Diszházi G, Almássy J, Madácsy T, Varga Á, Csernay-Biró P, Katona X, Tóth E, **Molnár R**, Rakonczay Z Jr, Hegyi P, Maléth J. TRPM2-mediated extracellular Ca^{2+} entry promotes acinar cell necrosis in biliary acute pancreatitis.
J Physiol. 2020 Jan 9; doi: 10.1113/JP279047
[IF_{2018}: 4.95]

Articles not related to the subject of the thesis:

I. Tuboly E*, **Molnár R***, Tőkés T, Turányi RN, Hartmann P, Mészáros AT, Strifler G, Földesi I, Siska A, Szabó A, Mohácsi Á, Szabó G, Boros M. Excessive alcohol consumption induces methane production in humans and rats.
Sci Rep. 2017 Aug 4; doi: 10.1038/s41598-017-07637-3.
[IF_{2018}: 4.122]

II. Varga G, Ugocsai M, Hartmann P, Lajkó N, **Molnár R**, Szűcs S, Jász DK, Érces D, Ghyczy M, Tóth G, Boros M. Acetylsalicylic acid-tris-hydroxymethyl-aminomethane reduces colon mucosal damage without causing gastric side effects in a rat model of colitis.
Inflammopharmacology. 2018 Feb; doi: 10.1007/s10787-017-0354-z.
[IF_{2018}: 3.838]

III. Béla Kovács, **Réka Molnár**, Előd Ernő Nagy, Éva Katalin Kelemen, Blanka Székely-Szentmiklósi, István Székely-Szentmiklósi, Boglárka Kovács-Deák and Árpád Gyéresi. Development and Validation of an UV-Spectrophotometric Method for the Assay of Strontium Ranelate and HPLC Stability Testing from Bulk and Pharmaceutical Dosage Form.
Acta Medica Marisiensis 2019; doi: 10.2478/amma-2019-0014
[IF_{2018}: 0.21]

Number of full publications: 5 (2 first author)

Cumulative impact factor: 16.80

CONTENTS

LIST OF FULL PAPERS RELATED TO THE THESIS 2
CONTENTS 3
LIST OF ABBREVIATIONS 4
1. INTRODUCTION 6
1.1. Physiology of ductal HCO_3^- secretion 7
1.2. Pathophysiological role of ductal HCO_3^- secretion 8
1.3. Limitations of in vitro and in vivo models 9
1.4. Organoid cultures 10
2. AIM OF THE STUDY 13
3. MATERIALS AND METHODS 14
3.1. Animals 14
3.2. Isolation of pancreatic ductal fragments 14
3.3. Pancreatic ductal organoid culture 15
3.4. Production of conditioned media and cell culture 16
3.5. Gene expression analysis 16
3.6. Fluorescent measurements in ductal fragments and organoids 17
3.7. Immunofluorescent labeling 19
3.8. Electron microscopy 19
3.9. Data Analysis 20
4. RESULTS 21
4.1. Establishment of mouse ductal epithelial organoid cell culture 21
4.2. mRNA expression patterns of ion channels and transporters in OCs and ductal fragments 21
4.3. The apical HCO_3^- secretion in ductal fragments and organoids 24
4.4. Indirect measurement of CFTR activity in pancreatic OCs using fluorescent Cl^- indicator. 26
4.5. Comparison of basolateral HCO_3^- uptake in isolated ducts and pancreatic organoids 28
4.6. Measurement of intraluminal pH in pancreatic organoids 29
4.7. Morphological and functional polarity of pancreatic OCs 31
4.8. Use of pancreatic organoids in pathophysiological studies 33
5. DISCUSSION 35
6. SUMMARY 40
7. NOVEL RESULTS AND OBSERVATIONS 42
8. ACKNOWLEDGMENT 43
9. REFERENCES 45

LIST OF ABBREVIATIONS

PDE: Pancreatic ductal epithelia
CFTR: Cystic fibrosis transmembrane conductance regulator
Cl^-: Chloride ion
VIP: Vasoactive intestinal peptide
Ach: Acetylcholine
NHE1: Na^+/H^+ exchanger 1
NBCe1: Electrogenic Na^+/HCO_3^- cotransporter 1
Na^+: Sodium ion
SLC26: Solute carrier family 26
SLC9: Solute carrier family 9
CO_2: Carbon dioxide
pHi: Intracellular pH
WNK/SPAK kinase: With-no-lysine/ SPS1-related proline/alanine-rich kinase
IRBIT: Inositol 1,4,5-trisphosphate receptor-binding protein
AP: Acute pancreatitis
CP: Chronic pancreatitis
CDC: Chenodeoxycholate
ER: Endoplasmic reticulum
SERCA: Sarco-endoplasmic reticulum calcium pump
ROS: Reactive oxygen species
TRPM2: Transient potential melastatin-like 2
iPCS: Induced pluripotent stem cells
OCs: Organoid cultures
LGR5: Leucine-rich repeat-containing G-protein coupled receptor 5
EGF: Epidermal growth factor
BMP: Bone morphogenetic protein
RSPO: R-spondin
Wnt: Wingless-related integration site
LRP5/6: Low-density lipoprotein receptor-related protein 5/6
E3: Ubiquitin ligase
RNF43: Ring finger protein 43
ZNRF3: Zinc and RING finger 3
FZD: Frizzled
KO: Knock-out
WT: Wild type
mRNA: Messenger ribonucleic acid
PCR: Polymerase chain reaction
SEM: Scanning electron microscope
DMEM: Dulbecco's Modified Eagle Medium
FBS: Fetal bovine serum
G-418: Geneticin-418 selection reagent
RT-PCR: Reverse transcription polymerase chain reaction
cDNA: Complementary deoxyribonucleic acid
HEPES: 4-2-hydroxyethyl)-1-piperazineethanesulfonic acid
HBSS: Hanks' Balanced Salt solution
BCECF-AM: 2',7'-Bis-(2-Carboxyethyl)-5-(and-6)-Carboxyfluorescein, Acetoxymethyl Ester
MQAE: N-(Ethoxycarbonylmethyl)-6-Methoxyquinolinium Bromide

$[Cl^-]i$: Intracellular chloride
NO_3^-: Nitrate ion
Fura-2-am: Fura-2-acetoxymethyl ester
SNARF-1: Seminaphtorhodafluor-1-acetoxymethylester
PFA: Paraformaldehyde
TBS: Tris(hydroxymethyl)aminomethane buffered saline
PBS: Phosphate-buffered saline
BSA: Bovine serum albumine
NH_4Cl: Ammonium chloride
NH_3: Ammonia
H^+/K^+ ATPase: Hydrogen potassium adenylpyrophosphatase
NKCC: $Na^+/K^+/Cl^-$ symporter
KCNA: Potassium voltage-gated channel subfamily a member
ANO1 or TMEM16A: Ca^{2+}-activated Cl^- channel Anoctamin1
BK channel: Ca^{2+}-activated K^+ channel
ENaC: Epithelial sodium channel
Clcn: Voltage-gated Cl^- channel
$[J(B^-)]$: Base flux
cAMP: Cyclic adenosine monophosphate
ATP: Adenosine triphosphate
PKA: Protein kinase A
S0859: N-cyanosulphonamide inhibitor of sodium-bicarbonate cotransport
EIPA: Ethylisopropyl amiloride
Kv: Voltage-gated potassium channel
ROS: Reactive oxygen species

1. INTRODUCTION

The pancreas is a complex organ that has exocrine and endocrine parts. The exocrine pancreas consists of two main cell types: acinar and ductal cells and has a tree-like structure formed by pancreatic ductal epithelial cells and pancreatic acinar lobes [1]. Acinar cells are responsible for the synthesis and secretion of pancreatic digestive enzymes [2]. The digestive enzymes are delivered from the acinar cells into the lumen at the terminal ends of the ductal branches [1]. The pancreatic ductal system have three segment: the main duct, interlobular and intralobular ducts [3, 4]. The pancreatic ductal epithelia (PDE) secretes bicarbonate-rich fluid upon secretin stimulation [5], which washes out the digestive enzymes from the ductal system and neutralizes the acidic pH of the gastric juice in the duodenum [6]. The alkaline pH of the pancreatic juice is determined by the secretion of HCO_3^-, which is exceptionally high in humans and reaches 140mM in the distal parts of the ductal system [7-10], whereas in mice and rats the maximal HCO_3^- concentration is only ~50-70 mM [11]. The ductal epithelia consists of polarized cells since the proteins, involved in the ion and fluid secretion show a polarized expression pattern on the apical and basolateral surfaces [3]. Due to the tight junctions the paracellular fluid and ion transport is limited [7, 10, 12] as described by Figure 1.

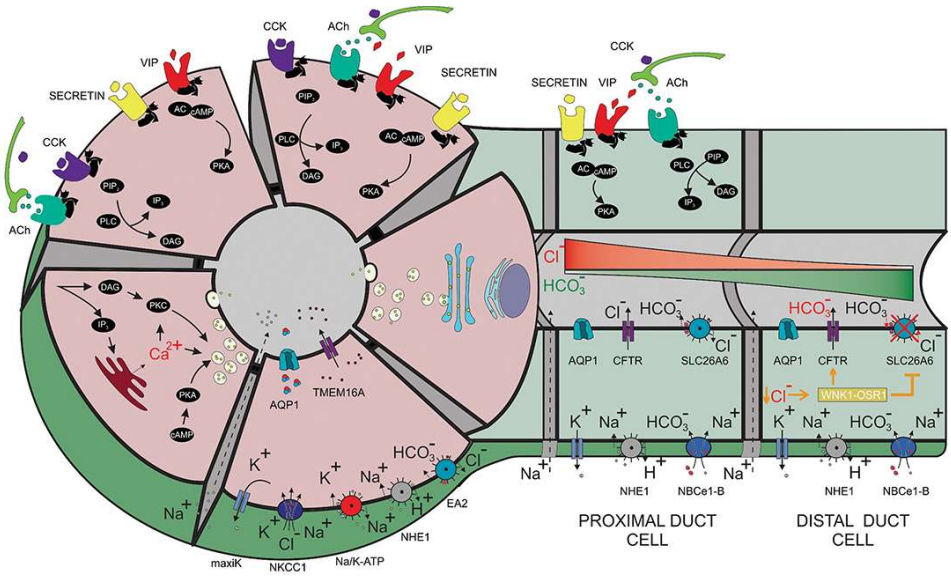

Figure 1. The molecular mechanism and regulation of HCO_3^- secretion in the exocrine pancreas. The pancreatic ductal cells accumulate HCO_3^- ions via the basolateral Na^+ -dependent membrane transporters. The HCO_3^- is then secreted across the apical membrane by the electrogenic Cl^-/HCO_3^- exchangers and cystic fibrosis transmembrane conductance regulator (CFTR) channel. The neurohormonal regulation of HCO_3^- secretion involves secretin, VIP and ACh. ***Schematic depiction: Jurij Dolensek et al. (2017). Pancreas Physiology. Challenges in Pancreatic Pathology. doi:10.5772/65895***

1.1. Physiology of ductal HCO_3^- secretion

As mentioned above, HCO_3^- ions are accumulated in the cells by two different mechanisms: through the Na^+-HCO_3^- cotransporter (NBCe1-B), or with passive diffusion of CO_2 entering the cell. CO_2 is converted to carbonic acid by the carbonic anhydrase enzyme, which is then hydrolyzed to HCO_3^- and H^+ in the cytosol [13]. The protons are secreted by the Na^+/H^+ exchanger (NHE) located on the basolateral side, whereas the HCO_3^- ions are secreted into the lumen [14]. The NBCe1-B cotransporter facilitate the entry of HCO_3^- in the cytosol through the basolateral membrane, during this process Na^+ gradient is utilized. NHE is a member of the SLC9 gene family, which is a subfamily of the monovalent cation-proton antiporter superfamily and similarly to the NBCe1-B, NHE is a Na^+ dependent transporter as well [15, 16]. NHEs are involved in several physiological processes, most importantly maintaining the intracellular pH by transporting H^+ to the extracellular space. Therefore as an antiporter NHE supports the basolateral HCO_3^- accumulation in the cytosol by providing driving force to the Na^+ dependent HCO_3^- uptake [14, 17].

The transporters and channels which are producing the nearly 140mM HCO_3^- rich juice on the luminal side are the Cl^-/HCO_3^- exchangers (members of the SLC26 transporter family) and cystic fibrosis transmembrane conductance regulator (CFTR). Previously, CFTR was only considered as a Cl^- channel providing the luminal Cl^- for the Cl^-/HCO_3^- exchange. However it is now generally accepted as a key contributor to the HCO_3^- secretion as well [12, 14, 15, 17, 18]. In this process the HCO_3^- permeability of CFTR, which is regulated by the WNK/SPAK kinase pathway sensitive to intracellular Cl^- [19] and by IRBIT, which coordinates basolateral HCO_3^- uptake and CFTR activity [20] and mediates synergy between Ca^{2+} and cAMP signaling [21]. The transporters and mechanism of HCO_3^- secretion is summarized in Figure 2.

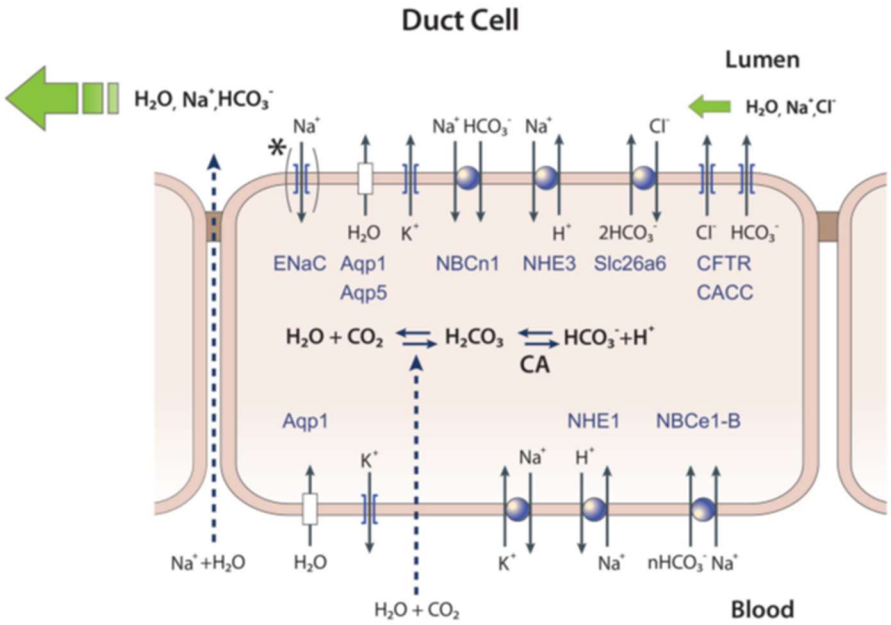

Figure 2. Schematic depicting the mechanism of ductal fluid and bicarbonate secretion. Several transporters mediate bicarbonate secretion in epithelial cells. Na^+/ HCO_3^- cotransporter (NBC) in the basolateral membrane absorb bicarbonate from the blood. NHE maintain the intracellular normal pH by transporting H^+ to the extracellular matrix. Electrogenic Cl^-/ HCO_3^- exchangers and CFTR channel secrete HCO_3^- rich fluid in the lumen. ***Schematic depiction: Lee M.G. et al. Physiol Rev. 2012 Jan;92(1):39-74.***

1.2. Pathophysiological role of ductal HCO_3^- secretion

Pancreatic ducts play an essential role in several pancreatic diseases like cystic fibrosis and acute or chronic pancreatitis [22]. Acute pancreatitis (AP) is an inflammatory disorder of the pancreas, which is the most common cause of hospitalization among non-malignant gastrointestinal diseases and has currently no specific therapy. Research in recent years has provided evidence that the failure of pancreatic ductal HCO_3^- secretion leads to increased severity of AP [23, 24]. Previously, our group investigated the changes of the ductal HCO_3^- secretion in different pathological AP models, such as biliary and alcohol-induced experimental AP [10, 23, 24]. In biliary AP Venglovecz et al showed that the non-conjugated bile acid, chenodeoxycholate (CDC), dose-dependently affects the HCO_3^- secretion in ductal epithelial cells, in low concentration (100µM) CDC stimulated, whereas in high concentration (1mM) inhibited the apical HCO_3^- efflux [25]. The mechanism involved sustained intracellular Ca^{2+} overload [25] and mitochondrial damage leading to intracellular ATP depletion [10, 13]. The sustained intracellular Ca^{2+} overload in isolated ductal cells was triggered by bile acids by the IP_3 receptor-dependent release of intracellular Ca^{2+} stores and inhibition of the ATP-dependent

reuptake of Ca^{2+} by sarco-endoplasmic reticulum Ca^{2+} pump (SERCA) [26] and activation of the influx of extracellular Ca^{2+} [27].

Excessive alcohol consumption is the other most common cause of AP, which is responsible for ~30-40% of all cases [28, 29]. The ethanol and non-oxidative ethanol metabolites can induce similar intracellular changes in ductal epithelial cells like bile acids. In low concentration administration of ethanol stimulate the ion secretion of SLC26A anion exchangers and CFTR channel via phospholipase C and inositol triphosphate-mediated Ca^{2+} release from the endoplasmic reticulum (ER) [24, 29, 30]. On the other hand ethanol and the non-oxidative ethanol metabolites, like fatty acid ethyl esthers and fatty acids can induce sustained intracellular Ca^{2+} elevation, which lead to ATP depletion and necrosis [30, 31] and inhibit the fluid and HCO_3^- secretion of the ductal epithelia. Moreover, ethanol reduces mRNA expression of the CFTR in pancreatic ductal cells, that contributes to the decreased HCO_3^- secretion [24].

The role of the ductal cells in the pathological mechanism is becoming increasingly accepted. Therefore, to understand the development and course of pancreatitis, it is essential to detect changes in the ductal cell and to detect changes in HCO_3^- secretion. Understanding the mechanism can contribute to the development of the therapy of this disease.

1.3. Limitations of in vitro and in vivo models

Several *in vitro* and in *vivo* models were applied to investigate physiology and disease mechanism in the exocrine pancreas. Molecular mechanisms of ductal secretion are well characterized on 2D cell cultures and in isolated ductal fragments, which is a classic model to study pancreatic exocrine secretion. The pancreatic ductal cell lines are derived mostly from human pancreatic tissue samples and are popular since they require relatively easy culture conditions and allow high throughput studies. However, most of them have been established from pancreatic ductal adenocarcinoma (such as CFPAC-1, Capan-1, or Capan-2), these cell lines were utilized in studies of ion transport processes of the pancreatic ductal epithelia in the past decades [32]. The human cystic fibrosis pancreatic ductal cell line allows to investigate the HCO_3^- secretion defect of CFTR channel [33]. Although these cell lines are useful for the physiological and pathophysiological studies of ductal epithelial cells, due to their tissue of origin (usually adenocarcinoma) they fail to mimic the morphology of epithelial cells, especially apical-basal polarity, whereas the expression of functional proteins, such as ion channels and transporters are different as well. As a result of these, 2D cell lines are not suitable to study exocrine pancreatic physiology and pathology [34]. Moreover, 2D cell lines

accumulate multiple culture-induced mutations or contamination with other cell lines over time in culture conditions, that limit their value as accurate models for disease modelling [35].

Standard isolation techniques of pancreatic ducts [8] - based on digestion of the pancreas with collagenase and manual isolation of the ductal fragments under stereomicroscope - have been used extensively to study pancreatic ductal physiology and pathology and led to a better understanding of the ductal epithelia in health and disease. This technique made the study of primary PDE cell possible, including physiologically relevant measurements, such as forskolin induced swelling [23] or fluorescent indicator-based intracellular pH measurements [6]. The most important limitation of this widely used isolation technique is that the complete removal of the surrounding conjunctive tissue – including fibroblasts – is not possible under a stereomicroscope leading to a mixed culture of epithelial and mesenchymal cells [13]. Thus, for example evaluation of changes in gene expression of epithelial cells could be confounded by alterations in the surrounding fibroblasts. Moreover, due to the limited amount of the isolated tissue studies of protein expression is limited to immunofluorescent labeling, whereas, the applicability of other techniques to study protein expressions are limited and difficult. Although animal models are more physiological and overcome this limitation, the differences of species-specific gene regulations are a huge drawback to use them for studying human disease. Another problem is that genome editing and manipulation of niche components are limited in the *in vivo* models [34]. In addition, the generation of proper animal models is time consuming, it usually takes 6-12 months and have therefore extremely limited throughput.

Therefore, to overcome current limitations of pancreatic research, we need novel models to study physiology, pathophysiology and possible drug treatments in translational pancreatic research. The requirement of this novel model system are as follows: morphological and functional similarity to primary pancreatic tissue, genome stability, but also keep all benefits of 2D cultures, such as monolayer expansion, easy genome manipulation, and the possibility to be sustained for long time storage to be preserved in biobank. Organoids, a novel model in the gastrointestinal research fulfill these requirements and this model is an important bridge between *in vitro* and *in vivo* animal or human model [34].

1.4. Organoid cultures

Over the last twenty years, a variety of three-dimensional (3D) cultures have been developed to study normal non-transformed cells [36-41] as Figure 3 represent. Organoid cell cultures (OCs) can be established from embryonic stem cells and from induced pluripotent stem cells

(iPSC) [42]. These culture techniques result in mixed cultures that contain epithelial and mesenchymal cells as well. Another culture technique utilizes tissue specific Leucine-rich repeat-containing G-protein coupled receptor 5 positive (Lgr5+) adult stem cells, which was a major breakthrough that allows researchers to produce cultures and maintain from hard-to-reach cells such as pancreatic or liver epithelial cells [41, 43, 44].

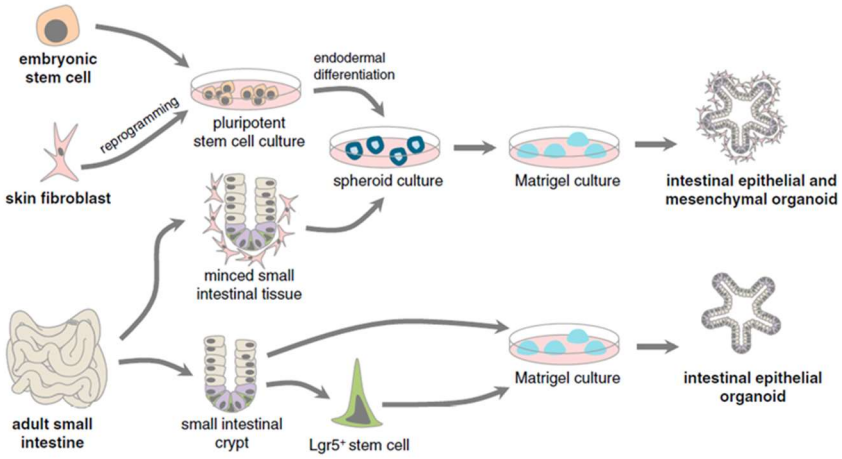

Figure 3. Developing of organoid cultures from different cell type. Pancreas epithelial adult stem cells express LGR5 markers, therefore stimulation of Wnt (Wingless-related integration site) signaling pathway generate cell division, which result organoid culture. ***Schematic depicting: Kretzschmar K. et al. Dev. Cell. 2016.***

Organoid cultures (OCs) derived from tissue specific Lgr5+ adult stem cells emerged recently as novel models of organ development and disease [41, 44]. By maintaining the activity of Wnt/β-Catenin signal transduction cascade – a key driver of most types of tissue stem cells [45] - OCs can be grown *in vitro* for long-term in 3D extracellular matrix based hydrogels; whereas, epithelial cells in the culture maintain the original cellular diversity and organization of the organ of origin [39]. The technique was originally developed to culture small intestinal Lgr5+ adult stem cells that generated crypt–villus like structures [40]. Since then OCs have been established from a wide range of organs in the gastrointestinal tract, including large intestine and esophagus [44], stomach [46], liver and pancreas [36]. Clear advantages of OCs over conventional 2D cell cultures are that in OCs more relevant cell-to-cell contact is maintained, whereas in 2D cultures the cells are attached to the plastic surface and cell-to-cell contacts are limited to the edges [37]. In pancreatic research currently OCs are studied as relevant human models of tissue development [1] and carcinogenesis [38]. The above described potential limitations of isolated ductal fragments might be overcome by the application of pancreatic

OCs for both physiological and pathological studies. However, the physiological relevance of pancreatic OCs is currently not known.

As mentioned above, the generation of adult stem cell derived OCs rely on the maintenance of the Wnt/ β-Catenin signal transduction cascade. Wnts are fundamental drivers of tissue stem cells in adult mammals. In the absence of Wnt β-Catenin gets phosphorylated and degraded thus the expression of β-Catenin regulated genes is inhibited. In the signaling cascade extracellular Wnt proteins bind to a receptor complex of two molecules, FZD and LRP5/6 (Figure 4.). This mechanism would lead to a conformational change of the receptors, which then in a complex mechanism that involve several proteins leads to the prevention of β-Catenin degradation thus β-Catenin can enter the nucleus and facilitate gene transcription. Another component of the pathway is the Wnt agonists R-spondins (Rspo) that interact on the cell surface with members of the LGR5 family to enhance Wnt signaling. Wnt signaling pathway plays crucial role in multiple cellular processes such as stem cell maintenance and cell fate decision [45]. On the other hand dysfunction of Wnt signaling pathway lead to several diseases including cancer and metabolic disorders [47, 48]. The Wnt signal transduction is summarized in Figure 4.

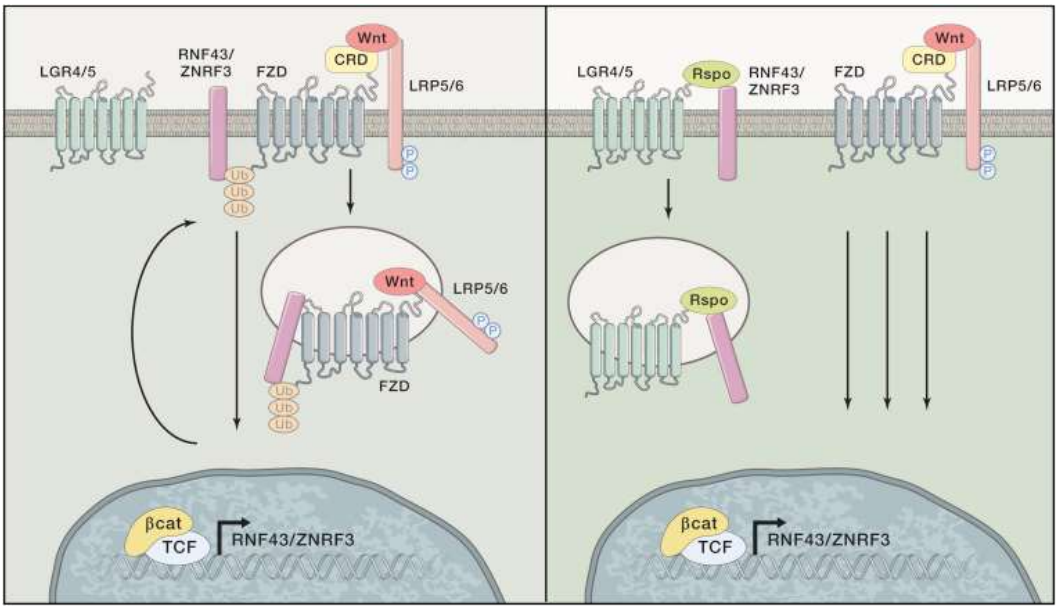

Figure 4. Wnt-agonist RSPOs enhance Wnt signaling pathway by LGR5. **A.** Membrane-bound E3 ubiquitin ligases RING finger 43 (RNF43) and zinc and RING finger 3 (ZNRF3) suppress Wnt transduction by removing Frizzled (FZD) receptors from the cell surface. **B.** R-spondin complex with LGR5 and RNF43/ZNRF3 neutralize the Wnt negative feedback activity and enhance the canonical Wnt signaling [49]. ***Schematic depicting: Nusse R, Clevers H. Cell 2017 Jun 1;169(6):985-999.***

2. AIM OF THE STUDY

Our aims in this project were

- to establish ductal epithelial organoid cell culture from mouse pancreatic ductal cells

- to compare the morphology and function of ductal epithelial cells in pancreatic OCs and in isolated pancreatic ductal fragments that is a standard model of exocrine pancreatic physiology

- to characterize the effect of bile acid on pancreatic ductal organoids and examine the Ca^{2+} release in TRPM2 konck-out (KO) ductal fragments compared to wild type (WT)

3. MATERIALS AND METHODS

3.1. Animals

10-12-week-old FVB/N mice were used to compare the morphology and function of epithelial cells in primary pancreatic ductal fragments and organoids. TRPM2 knockout mice were generously provided by Yasuo Mori (Kyoto University; Kyoto, Japan). The knockout mice were generated from a C57BL/6 background as described previously [50]. $TRPM2^{+/+}$ and $TRPM2^{-/-}$ mice were bred from $TRPM2^{+/-}$ animals and were used for experiments between the age of 8–12 weeks. Mice were kept in standard 12 hour light-dark cycle and on standard rodent food ad libitum. Mice were genotyped using a standard polymerase chain reaction (PCR) assay as described in Liu *et al.* [51]. Experiments on live animals were carried out with adherence to the NIH guidelines and the EU directive 2010/63/EU for the protection of animals used for scientific purposes. The study was authorized by the National Scientific Ethical Committee on Animal Experimentation under license number XXI./2522/2018 for the FVB/N mice and XXI./2523/2018 for the TRPM2 knockout mice.

3.2. Isolation of pancreatic ductal fragments and acinar cells

Pancreatic ductal fragments. Mice were sacrificed by terminal anesthesia and the pancreatic tissue was removed and placed into wash media (Table 1.) kept on ice. The tissue was cleaned from fat and lymph nodes. The tissue was then digested with 100 U/ml purified collagenase (Worthington), 0.1 mg/ml trypsin inhibitor (ThermoFisher Scientific) and 1 mg/ml bovine serum albumin (BSA; VWR) in DMEM at 37°C for 30 min. After digestion, the supernatant was removed and the tissue was placed in a 15 mL Falcon tube with cold 10 mL wash media and was divided to multiple pieces. Small intra-/interlobular ducts were then isolated by microdissection under stereomicroscope and were used for measurements on the same day. The composition of splitting and wash media is described in Table 1.

Mouse Spliting Media			
Name	**Producer**	**Catalog number**	**Final concentration**
Advanced DMEM F12	ThermoFisher	12634010	
HEPES	ThermoFisher	15630080	10mM
Penicillin/Sterptomycin	ThermoFisher	15140122	10mM
GlutaMAX	ThermoFisher	35050061	10mM

Mouse Wash Media	
Name	**Final concentration**
Mouse Splitting Media	
FBS	2,5% (V/V)

Table 1. Composition of the splitting and wash media.

Pancreatic acinar cells. TRPM2 WT acinar cells were isolated based on Gout *et al.* 2013 [52]. Mice were sacrificed by terminal anesthesia and pancreas was removed into ice-cold Hank's balanced salt solution (HBSS; Sigma-Aldrich). Lymph nodes and fat were removed and pancreas was cut to small pieces. Small pancreas pieces were placed into a sterile flask with 10 ml of isolation solution (10 ml HBSS, 200 U/ml collagenase, Worthington, 10mM HEPES, Sigma-Aldrich). For the digestion, tissue was transferred to T25 flask at 37°C for 25-30 min and were shaken in every 5 minutes. After the digestion the tissue was transferred in 50 mL tube and was added 10 ml of ice-cold washing solution (containing 10 ml HBSS, 10 mM HEPES, 5% fetal bovine serum (FBS), Gibco) and was centrifuged at 90 relative centrifugal force (RCF) at 4°C for 2min. After the centrifuge, supernatant was removed and pellet was suspended with 1 ml HBSS solution. Acinar cells were kept at 37°C with 5% CO_2 until the using.

3.3. Pancreatic ductal organoid culture

To establish pancreatic organoid cultures (OCs), 8-12 weeks old FVB/N mice (20-25g bw) were used. The ductal fragments were isolated as described above and were cultured in Matrigel (Corning) covered with 2 mL complex organoid Feeding Media (Table 2.) in a standard 35 mm petri dish at 37°C with 5% CO_2. The organoids were passaged every 7 days by gentle pipetting.

Mouse Feeding Media			
Name	**Producer**	**Catalog number**	**Final concentration**
Mouse Splitting Media			
A83-01	Tocris	2939	500nM
EGF Recombinant Mouse Protein	ThermoFisher	PMG8041	50ng/ml
Recombinant Human FGF-10	Shenadoah Biotechnology	100-183	100ng/ml
Gastrin I	Tocris	3006	0.01μM

mNoggin conditioned media			(0,1% V/V)
N-acetylcysteine	Sigma-Aldrich	A9165-5G	1.25mM
Nicotinamide	Sigma-Aldrich		10mM
recombinant R-Spondin	R&D Systems	4645RS-100	
B27 Supplement 50X serum free	ThermoFisher	17504044	1X
Y-27632 Rho-kinase inhibitor	Tocris	1254/1	10.5µM
Prostaglandin E2	R&D Systems	2296/10	1 µM
Wnt-3A conditioned Media from L Wnt-3A Cells	ATCC	CRL-2647	50% (V/V)

Table 2. Composition of the mouse feeding media.

3.4. Production of conditioned media and cell culture

Conditioned media was produced by the L-Wnt-3A expressing cell line was purchased from ATCC (CRL-2647), Cultrex HA-R-Spondin1-Fc 293T cell line was from Trevigen and Noggin producing cell line was a kind gift from Hans Clevers (Hubrecht Institute, Utrecht, The Netherlands). All cell lines were grown in a selection media according to the manufacturer's instructions. Briefly, L-Wnt-3A was grown in Dulbecco's modified Eagle medium (DMEM) Nutrient Mixture F-12 Ham (Sigma, 6421), HA-R-Spondin-Fc 293T in DMEM high glucose (Gibco), Noggin HEK-293 in DMEM high glucose and sodium pyruvate (Gibco). The media were supplemented with 10% FBS, 1% Penicillin/Streptomycin and 0.4 mg/ml Geneticin-418 (Sigma-Aldrich) selection reagent (G-418). Conditioned media were generated without G-418 for one week.

3.5. Gene expression analysis

The mRNA expression of OCs and primary isolated ductal fragments was carried out by conventional combining reverse-transcription (RT-PCR) and conventional polymerase chain reactions (PCR). Total mRNA was purified by NucleoSpin RNA XS kit (Macherey-Nagel) according to the manufacturer's instructions from 3 independent biological replicates of mouse whole brain tissue, mouse ductal fragments, or OCs. The mRNA concentrations were verified by NanoDrop™ 2000 spectrophotometer (ThermoFisher Scientific). 1 µg purified mRNA was used for each cDNA synthesis step. RT-PCRs were carried out by using iScript™ cDNA Synthesis kit (Bio-Rad). For the conventional PCR amplification DreamTaq Hot Start DNA Polymerase (ThermoFisher Scientific) and cDNA specific primers were applied. All the primers were validated on template cDNA derived from mouse brain tissue. To compare gene

expression levels, we used plot lanes analysis quantification by ImageJ software. Applied specific primer is described in Table 3.

Gene	Target NCBI	Primers (Fwd, Rev)	Lengh	Binding position	Tm	GC%	Product (bp)
Cftr	NM_021050.2	TAGGGGAAGTCACCAAGGCT	20	406-425	60,18	55	152
		TGGGTGAAGAAGCAGTGTCC	20	557-538	59,89	55	
Slc9a1	NM_001358455.1	GACCCACTGGCCTATGAACC	20	3092-3111	60,11	60	109
		TGCCCTTCAACTCCTCGTTC	20	3200-3181	59,97	55	
Slc4a4	NM_001359211.1	GCCTACTGAAGCCTGACCTG	20	647-666	60,11	60	155
		TCGGGCATTATCAGGGTTGC	20	801-782	60,47	55	
Slc26a6	NM_134420.4	GAGCTGTTTGCAACGCTTGT	20	1788-1807	60,25	60	121
		CCTGGTTACTGTCCACACGG	20	1908-1889	60,32	60	
Ano1	NM_001242349	CCACTCTTCGCCCTGCTAAA	20	2429-2448	60,04	55	73
		TCCGTAGCTCGGTGACAAAC	20	2501-2482	60,04	55	
Atp12a	NM_138652.2	GCACCATCATGATCAACGGC	20	1802-1821	59,97	55	114
		GACAGAAACCCAACACACGC	20	1915-1896	59,97	55	
Scnn1a	NM_011324.2	CCAAGCACAACCGCATGAAG	20	849-868	60,39	55	193
		GTGTATCTGTAAGGATTAAGGGTGC	25	1041-1017	59,24	44	
Clcn1	NM_013491.2	CTACGGACTGCCCTCAGAGA	20	178-197	60,39	60	89
		ATATCTGTGTTGGGTGGGCAT	21	266-246	59,43	47,62	
Clcn3	NM_173874.1	GCATAACCAGCGCGAGTAGC	20	605-624	61,82	60	118
		TAATGAGTTCCAGCTGCTGTGT	22	722-701	59,96	45,45	
Kcnma1	NM_001253364.1	GTGGTAACGTGGACACCCTT	20	2266-2285	59,89	55	85
		TCAAAGGCACGGAAACTGGT	20	2350-2331	60,11	50	
Kcna1	NM_010595.3	AACGCATGCGCTACTTTGAC	20	2280-2299	59,83	50	143
		CTCGGAGAACATGTCCAGGG	20	2422-2403	59,82	60	
Kcna2	NM_008417.5	GACCTGTGAACGTGCCCTTA	20	980-999	59,97	55	99
		TGTAGCCTTCATCCTCCCGA	20	1078-1059	60,03	55	
Kcnd3	NM_001039347.1	CCAGTCGCTCCAGCCTTAAT	20	2171-2190	59,82	55	193
		ACCTTGACGACATTGCTGGT	20	2363-2344	59,89	50	
Kcnh1	NM_010600.3	GCTCCGATCAGGAACGAACA	20	571-590	60,11	55	103
		AACCTTTGCAGGAGTCGTCC	20	673-654	60,25	55	
Slc26a3	NM_021353.3	CTCGGACCCCAATGCTTCTT	20	647-666	60,04	55	127
		CCCCAGGAGCAACTGAATGA	20	773-754	59,67	55	
Slc12a2/5	NM_009194.3	CCATCGCCGACTTCGTCATA	20	1445-1464	59,97	55	115
		TCTCGAAAATCCGGCCCAAA	20	1559-1540	59,96	50	
Slc26a6/11	NM_134420.4	GAGCTGTTTGCAACGCTTGT	20	1788-1807	60,25	60	121

Table 3. Full list of primers used in the project.

3.6. Fluorescent measurements in ductal fragments and organoids

Pancreatic ductal fragments or organoids were attached to a poly-l-lysine coated coverglass and were incubated in standard HEPES solution with BCECF-AM (1.5µmol/L), Fura-2-AM

(5µmol/L), or MQAE (2µmol/L) for 30 n at 37°C. Cover glasses were then transferred to a perfusion chamber mounted on an Olympus IX71 inverted microscope. Dye loaded samples were excited with an Olympus MT-20 illumination system equipped with a 150 W xenon arc light source. For BCECF the filter combination was as follows: 434/17 nm and 497/16 nm single-band bandpass filters for excitation (Semrock; P/N: FF01-434/17-25 and FF01-497/16-25, respectively), 511 nm edge single-edge standard epi-fluorescence dichroic beamsplitter (Semrock; P/N: FF511-Di01-25X36) and 537/26 nm single-band bandpass filters for emission (Semrock; P/N: FF01-537/26-25). For Fura2: 340/26 nm and 387/11 nm single-band bandpass filters for excitation (Semrock; P/N: FF01-340/26-25 and FF01-387/11-25, respectively), 409 nm edge single-edge standard epi-fluorescence dichroic beamsplitter (Semrock; P/N: FF409-Di03-25x36) and 510/84 nm single-band bandpass filters for emission (Semrock; P/N: FF01-510/84-25). For MQAE: 340/26 nm single-band bandpass filters for excitation (Semrock; P/N: FF01-340/26-25), 409 nm edge single-edge standard epi-fluorescence dichroic beamsplitter (Semrock; P/N: FF409-Di03-25x36) and 510/84 nm single-band bandpass filters for emission (Semrock; P/N: FF01-510/84-25). The fluorescent signal was captured by a Hamamatsu ORCA-ER CCD camera trough a 20X oil immersion objective (Olympus; NA: 0.8) with a temporal resolution of 1 sec. Ratiometric image analysis was performed by Olympus excellence software.

Generation of intracellular ROS was measured by H2DCFDA ROS indicator (ThermoFisher Scientific). Isolated pancreatic acinar cells and ductal fragments were incubated with 4 µM H2DCFDA in standard HEPES solution for 20 min at 37°C on a poly-L-lysine-coated cover glass. H2DCFDA was excited at 490 nm and the emitted fluorescence was captured between 500 and 550 nm. Fluorescence signals were normalized to initial fluorescence intensity (F/F0) and expressed as relative fluorescence. For pH measurement with SNARF-1 (ThermoFisher Scientific), or SNARF-1 dextran (ThermoFisher Scientific) organoids were attached to a poly-l-lysine coated coverglass and were incubated in standard HEPES solution with SNARF-1 (10µM) for 30 min at 37°C. SNARF-1 dextran was injected into the lumen of the organoids using a glass injection pipette. Images were captured by a Zeiss LSM880 confocal microscope was used with a 40X water immersion objective (Zeiss, NA: 1.2). Samples were excited with 514 nm Argon laser and emitted fluorescent signal was captured by a GaASP detector between 550-580 nm and 610-650 nm respectively with a temporal resolution of 5 sec. The ratio of the two emission wavelength (640/580 Ratio) was calculated by Zeiss Zen Black software.

3.7. Immunofluorescent labeling

Isolated pancreatic ductal fragments or organoids were frozen after the first passage in Shandon Cryomatrix (ThermoFisher Scientific) and stored at -20°C until sectioning. 7 µm thick sections were cut with cryostat (Leica CM 1860 UV) at -20°C. Sections were fixed in 4 % PFA-PBS for 15 min then washed in 1x Tris buffered saline (TBS) for 3x 5 min. Antigen retrieval was performed in Sodium Citrate - Tween20 buffer (0.001M Sodium Citrate Buffer, pH 6.0 and 0.05% Tween20) at 94°C for 30 min. Sections were blocked with 0.1% goat serum and 10% bovine serum albumin (BSA)-TBS for 1 h. Incubation with primary antibodies were performed overnight at 4°C. For the list and dilution of antibodies, please see Table 4. Sections were incubated with secondary antibody for 2 h at room temperature. Nuclear staining was performed with 1 µg/ml Hoechst33342 (ThermoFisher Scientific) for 15 min and sections were placed in Fluoromount mounting medium (Sigma-Aldrich) then left to dry. Images were captured with a Zeiss LSM880 confocal microscope using a 40X oil immersion objective (Zeiss, NA: 1.4).

Antibody	Host	Clonality	Provider	Cat. No.
anti-CFTR	rabbit	Polyclonal	Alomone Labs	ACL-006
anti-SLC4A4	rabbit	Polyclonal	Abcam	ab187511
anti-NHE-1	rabbit	Polyclonal	Abcam	ab67313
Goat anti-Rabbit IgG, Alexa Fluor- 488	goat		ThermoFisher Scientific	A11034

Table 4. Full list of primary antibodies used in the project.

3.8. Electron microscopy

Sample preparation. Isolated pancreatic ductal fragments or organoids after the first passage were fixed for 24 h in 3% glutaraldehyde (Electron Microscopy Sciences) at room temperature and washed for 3x 15 min in 0.3M cacodylate buffer (pH 7.4) (EMS). For contrasting samples were incubated in 3% potassium ferrocyanide (Sigma-Aldrich) and 2% osmium tetroxide (EMS, Cat. No: 19110) in 300mM cacodylate buffer for 1 h at 4°C. This was followed by 20 min incubation in 1% thiocarbohydrazide (Sigma-Aldrich), then the samples were placed in 2% osmium tetroxide for 30 min at room temperature and finally samples were incubated overnight in 1% uranyl acetate at 4°C. Sample dehydration was performed with 20%, 50%, 70%, 96%

and absolute ethanol, respectively for 15 min in each dilution and 1,2-propylene oxide (Merck) was used as intermedier 2x 5 min. All solutions were prepared with AccuGENE molecular biology water (Lonza) and filtered through a 0.22 μm syringe filter. For infiltration Epon 812 resin was used according to the manufacturer's instructions (Embed 812 Resin, EMS, Cat. No.: 14900; DDS, EMS, Cat. No.: 13710, NMA, EMS, Cat. No.: 19000, BDMA, Sigma-Aldrich, Cat. No.: 185582). Sample infiltration was performed in two steps (propylene oxide + resin 1:1 solution then pure resin). Resin polymerization was done at 60°C for 24 hours.

Sectioning and imaging. Before sectioning, indium tin oxide covered glasses were put into a Quorum carbon coater (Quorum Q150R ES Plus, Quorum Tech) for negative glow discharge. The blocks were trimmed and 100 nm ultrathin sections were cut by a 35° Ultra jumbo diamond knife type (DIATOME) on an RMC Powertome ultramicrotome with 0.8 mm/sec cutting speed. Post contrasting was performed with 5% uranyl acetate and Reynolds solution. Sections were carbon-coated and placed into a Zeiss Sigma 300 scanning electron microscope (SEM). Images were captured by an in chamber secondary electron detector. Imaging parameters were as follows: 2.34 A filament current, 5 kV acceleration voltage. 30 nm pixel size was used for lower magnification and 10 nm for higher magnification images.

3.9. Data Analysis

All statistical analysis was performed using GraphPad prism. Data distribution was tested by Shapiro-Wilk test of normality. T-test was applied to compare two groups, one-way analysis of variance (one-way ANOVA) was applied to compare multiple groups in parametric, Mann-Whitney U test (rank sum test) was applied to compare two groups, Kruskal-Wallis (one-way analysis of variance on ranks) was applied to compare multiple groups in non-parametric, p values < 0.05 considered significant.

4. RESULTS

4.1. Establishment of mouse ductal epithelial organoid cell culture

First, we established and optimized 3D epithelial organoid cultures (OCs) from mouse pancreatic ductal fragments. The development of OCs was observed daily as demonstrated in Figure 5. Due to the intense proliferation of the ductal epithelial cells the formation of the bubble shape of OCs could be detected from day 2 in the Matrigel dome. By the end of the first week, the OCs reached maximal size, therefore OC passage was performed by mechanical disruption. The passage process resulted in small clusters and individual cells, which were embedded again in Matrigel. During the first passage conjunctive tissue and fibroblasts surrounding the basolateral side of the isolated ductal fragments was removed and pure epithelial cell OCs was established. The proliferation of cell was dependent on the Wnt signal molecule, therefore it had to be contained by the media. For the experiments, organoids were used until passage No. 5. to avoid any changes in gene expressions.

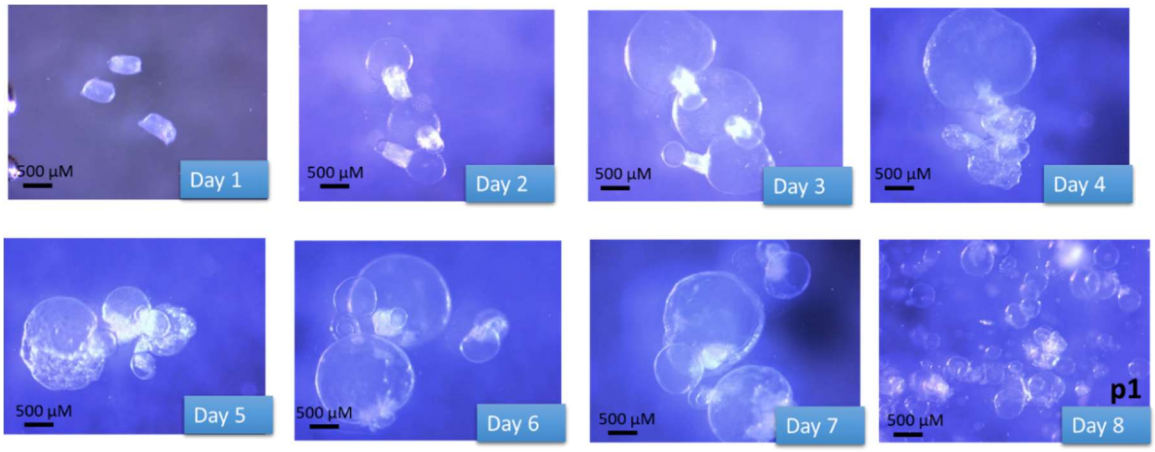

Figure 5. Expansion of pancreatic epithelial cells from primary tissue. The development was inspected every day at the same time, day 8 represents the first day after passage.

4.2. mRNA expression patterns of ion channels and transporters in OCs and ductal fragments

To confirm that OCs are suitable for studying pancreatic ductal secretion, similarities, and differences in gene expression patterns of ion channels and transporter proteins were investigated between isolated ducts and organoids. The list of investigated genes is provided in

Figure 6 A. Primers were validated with RT-PCR in isolated mouse brain tissue lysate with cycle numbers of 30 and 40, as shown in Figure 6 B.

A.

Gene name	Protein name
Slc9a1	Na^+/H^+ Exchanger 1 (NHE1)
SLC4A4	Electrogenic Na^+/HCO_3^- Cotransporter (NBCe1)
Slc26a6	Cl^-/Anion Exchanger (PAT-1)
Atp12a	H^+/K^+ ATPase (Nongastric)
Scnn1a	Epithelial Na^+ Channel
Clcn1/3	Cl^- voltage-gated channel 1/3
Kcnma1	Ca^{2+}-Activated K^+ Channel
Kcna1/2	Voltage gated K^+ Channel 1/2 (Subfamily A)
Kcnd3	Voltage gated K^+ Channel 3 (Subfamily D)
Kcnh1	Voltage gated K^+ Channel 1 (subfamily H)
Slc26a3	Cl^-/Anion Exchanger (DRA)
Slc12a2	Basolateral $Na^+/K^+/Cl^-$ Symporter

B.

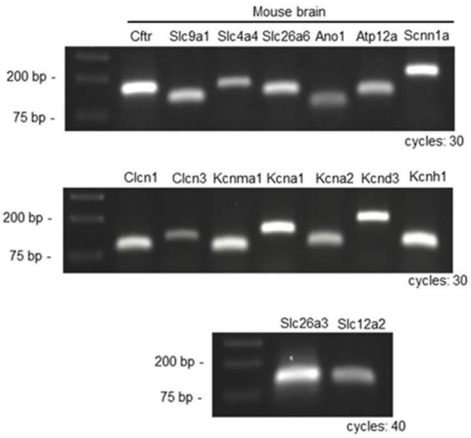

Figure 6. Comparison of gene expression of isolated pancreatic ducts and pancreatic organoids. **A.** Full list of key transporter genes and encoded proteins. **B.** Validation of primer specificity in mouse whole brain lysate in 30 and 40 cycles.

Gene expression of isolated ducts and organoids were investigated in 30 (Figure 7. A) and 35 (Figure 7. B) cycles. The gene expression patterns of the two samples markedly overlaped. Intensity values were higher after 35 cycles, therefore we choosed to use these values to assess relative band densities.

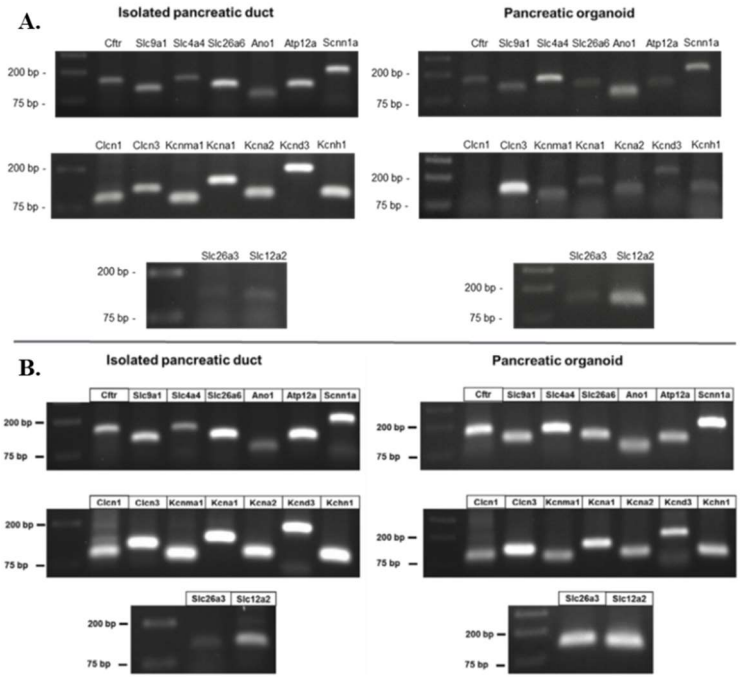

Figure 7. Gene expression analysis in OCs compared to isolated ductal fragments. Gel-electrophoresis representing RT-PCR with cycle numbers of 30 (**A**) and 35 (**B**).

Comparisons of relative band densities showing gene expression patterns within one gel are presented in Figure 8. Expression of Slc26a6, CFTR, NHE1 and NBCe1 was confirmed in both isolated ductal fragments and in pancreatic OCs. Furthermore, the expression of non-gastric H^+/K^+ ATPase; Ca^{2+}-activated K^+ channel (BK channel); Slc26a3 Cl^-/anion exchanger and the basolateral $Na^+/K^+/Cl^-$ symporter (NKCC) was also demonstrated. The expression of K^+ channels in the pancreatic ductal epithelium is controversial and species dependent [3] therefore, we selected four members of the voltage-gated subfamily Kcna1, Kcna2, Kcnd3 and Kcnh1, which were not yet described in the pancreatic ductal epithelium to further confirm the similarity of gene expression in primary ducts and OCs. Results show that all four members of the subfamily are expressed in both samples, further suggesting their potential uniformity. Interestingly, we also detected the expression of the genes encoding the epithelial sodium channel (ENaC), the Ca^{2+}-activated Cl^- channel Anoctamin1 (ANO1, or TMEM16A) and two members of the voltage-gated Cl^- channels (Clcn1 and Clcn3) in both isolated primary ductal fragments and pancreatic OCs.

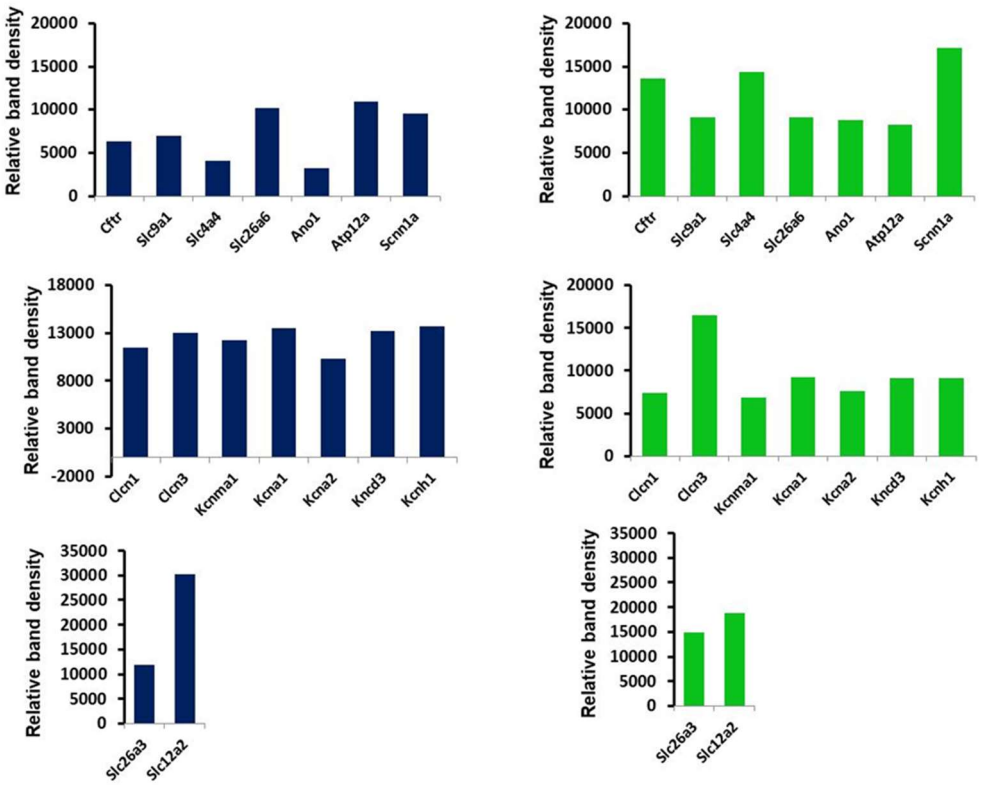

Figure 8. Relative band densities. Relative band densities show the comparison of gene expression of isolated pancreatic ductal and OCs by 35 cycle. Blue bar charts represent gene expression of isolated pancreatic ducts and green bar charts represent gene expression of pancreatic organoids.

4.3. The apical HCO_3^- secretion in ductal fragments and organoids

As the primary function of the ductal epithelia is ion (especially HCO_3^-) and fluid secretion, we used standard intracellular pH (pH_i) measurement based on the fluorescent pH indicator BCECF-AM to estimate the ion transporter activities to further confirm the functional similarity of OCs and isolated ducts. First organoids and ductal fragments were perfused with 20mM NH_4Cl in standard HEPES solution. As a result, the pH_i has markedly increased, since ammonia is able to diffuse trough the cell membrane, into the intracellular space, where it shifts the acid-base balance into an alkaline direction by proton depletion and the generation of HCO_3^-. After extracellular and intracellular ammonia concentrations are equalized, cells start to recover intracellular pH by secreting the generated HCO_3^-. This phase is defined as recovery from the alkali load. During this process HCO_3^- is secreted into the extracellular space trough the apical CFTR Cl^- channel and the SLC26A (3 and 6) anion exchanger. Removal of ammonia causes a rapid intracellular acidification due to the sudden increase of protons left behind by ammonia exiting the cells. For the regeneration from the acidosis, basolateral Na^+/H^+ antiporters are activated to remove protons, which increases the pH_i. The process is illustrated in Figure 9.

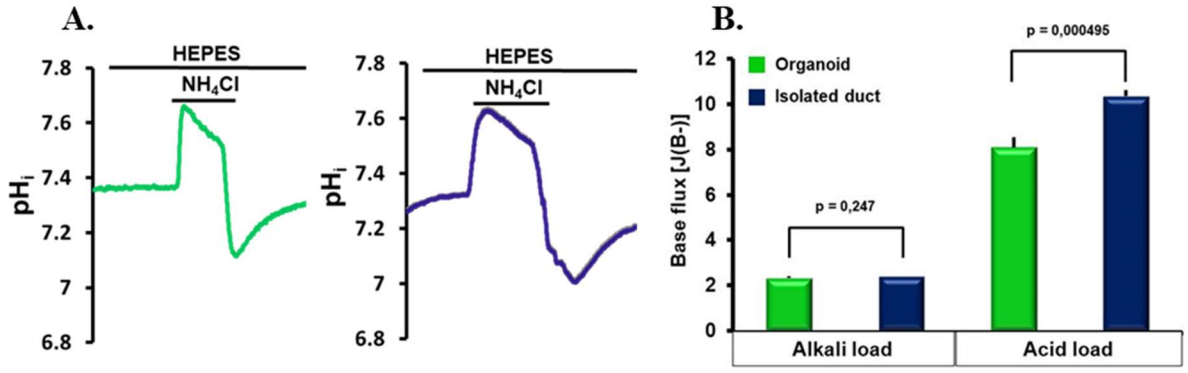

Figure 9. pH_i recovery of OCs and freshly isolated ductal fragments in standard HEPES solution. **A**. Representative traces showing intracellular alkalization by 20mM NH_4Cl administration. **B**. Bar charts showing the calculated base fluxes in standard HEPES solution. Recovery from alkalosis was minimal, as expected under these conditions, however recovery from acidosis was moderately but significantly higher in pancreatic ducts. Average number of experiments: n=4-6.

HCO_3^- secretion was further investigated with the basolateral administration of 20mM NH_4Cl in HCO_3^-/CO_2-buffered solution (Figure 10. A). Similarly, to the previous experiments, the pH_i immediately increased referring to the rapid diffusion of ammonia through the cell membrane followed by a slower regeneration from the alkali load. After the removal of NH_4Cl a rapid drop

in the pH_i was observed followed by the restoration of the resting pH_i. This recovery phase depends on activity of the basolateral NHE1, but due to the presence of the HCO_3^- under these conditions the basolateral Na^+/HCO_3^- cotransporter (NBCe1) is also active that facilitate HCO_3^- uptake. To quantify the recovery from alkalosis and acidosis, pH has been measured ($\Delta pH/\Delta t$) over the first 30 s and the base flux [J(B-)] was calculated as described in Maleth et al. 2015. With this approach, significant differences in the transport mechanisms in OC compared to isolated ductal fragments could not be observed (Figure 10. B). These results suggest that the activity of the apical Cl^-/ HCO_3^- exchanger and the basolateral HCO_3^- uptake is comparable.

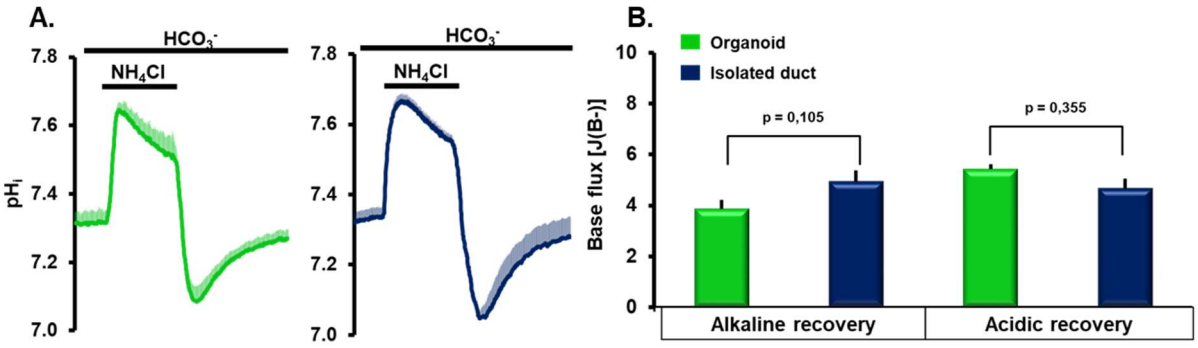

Figure 10. A. Bicarbonate secretion of OCs and freshly isolated ductal fragments in HCO_3^-/CO_2-buffered extracellular solution. Pancreatic ducts or organoids were alkalized with the administration of 20mM NH_4Cl. **B.** Bar charts showing calculated base flux of HCO_3^-/CO_2-buffered solution. Comparison of alkaline and acidic recovery, as representation of the apical and basolateral transport activities, showed no difference in primary ducts vs pancreatic organoids. Average number of experiments: n=4-6.

To assess the activity of CFTR and the contribution of the channel to HCO_3^- secretion in pancreatic ductal cells we treated isolated ducts and organoids with 10µM $CFTR_{(inh)}$-172, which is a specific inhibitor of the CFTR channel. The inhibitor was added during the NH_4Cl-pulse in HCO_3^-/CO_2 buffered solution as shown in Figure 11. A. Apical Cl^- dependent HCO_3^- secretion was decreased both in OCs and ductal fragments, compared to the controls shown in Figure 10. suggesting that CFTR participates in the mechanism of HCO_3^- secretion in both cell types. As demonstrated on the bar charts, exposure of the cells to CFTR inhibitor significantly decreased the base flux in both samples as shown in Figure 11 B.

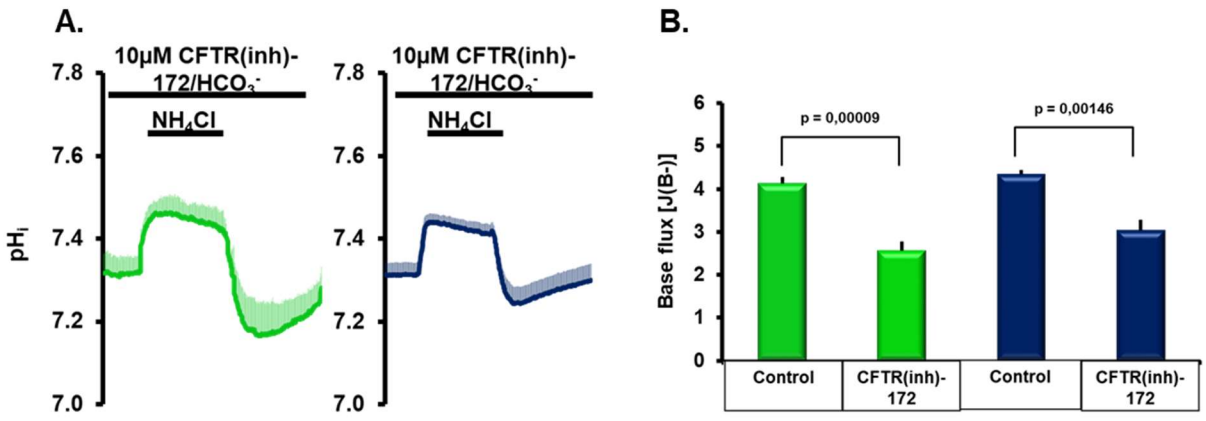

Figure 11. A. Inhibition of bicarbonate secretion with $CFTR_{(inh)}$-172 in OCs (green) and in freshly isolated ductal fragments (blue). Cells were perfused with HCO_3^-/CO_2-buffered extracellular solution and intracellular alkalization was induced with the administration of 20 mM NH_4Cl in the presence of $CFTR_{(inh)}$-172. **B.** Bar charts summarize the calculated base flux of alkaline recovery in the absence or presence of $CFTR_{(inh)}$-172. Comparison of alkaline recovery indicates the apical transport activities. CFTR inhibition markedly decreased alkaline recovery in OCs (green), as well in isolated ductal fragments (blue). Average number of experiments: n=4-6.

4.4. Indirect measurement of CFTR activity in pancreatic OCs using fluorescent Cl^- indicator

In this series of experiments, a Cl^- sensitive fluorescent indicator was used to measure $[Cl^-]_i$. The fluorescent signal of MQAE is quenched by Cl^- ions, therefore it is increased by the efflux of Cl^- from the intracellular matrix. Removal of extracellular Cl^- from the HCO_3^-/CO_2-buffered solution resulted in a decrease of $[Cl^-]_i$, most likely due to the Cl^- efflux from the cytosol via CFTR, which was significantly enhanced by Forskolin administration (Figure 12. A-C.). In addition, 10µM $CFTR_{(inh)}$-172 completely abolished the Cl^- extrusion, whereas the protein kinase A (PKA) inhibitor H-89 significantly impaired it to the non-stimulated control level further indicating that the measured Cl^- were due to the activity of CFTR. These results are consistent with our current knowledge of CFTR activity and regulation and thus this technique may be a powerful toolkit for researchers studying CFTR activity in 3D cultures.

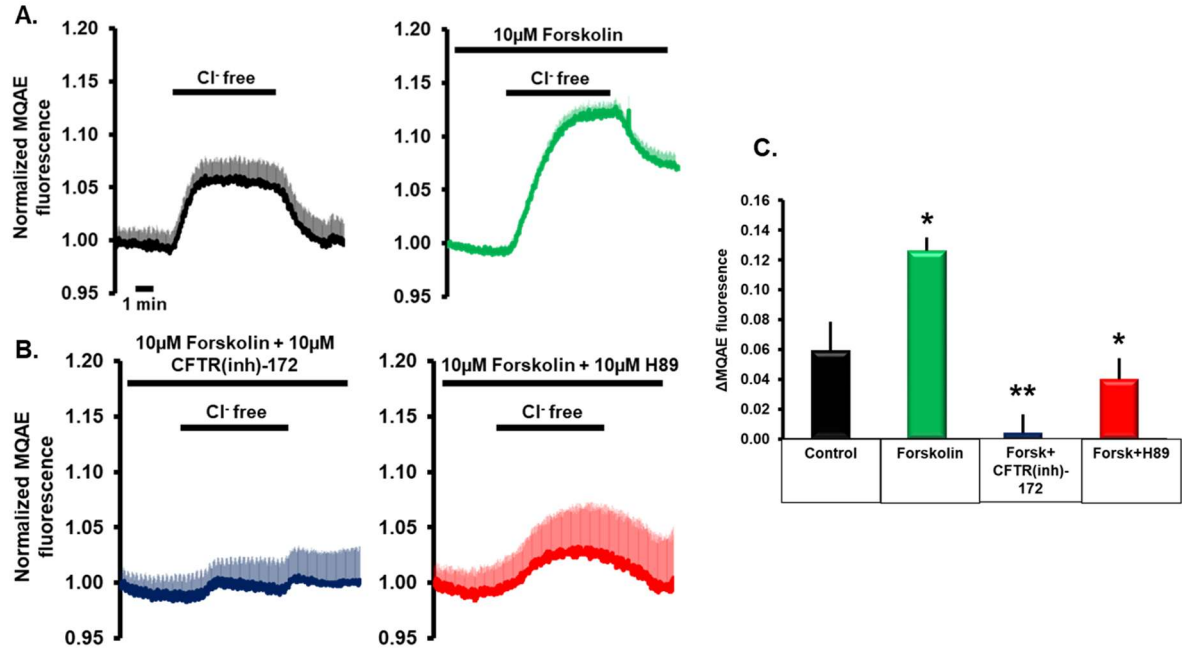

Figure 12. Pancreatic organoids were perfused with HCO_3^-/CO_2-buffered extracellular solution. Removal of extracellular Cl^- induced a drop in intracellular Cl^- levels, which were further decreased by the administration of 10µM forskolin (reflected by a remarkable increase in fluorescent intensity) due to the activity of CFTR. **B.** Inhibition of chloride secretion with 10µM $CFTR_{(inh)}$-172 completely abolished Cl^- efflux. The protein kinase A (PKA) inhibitor H-89 significantly impaired cAMP-stimulated CFTR activity in pancreatic organoids. **C.** Bar charts summarize the maximal fluorescent intensity changes. Average number of experiments: n=4-6.

We utilized this technique also to measure the activity of NKCC1 in isolated ducts and pancreatic organoids. As shown in Figure 13, the administration of 100 µM Bumetanide (an NKCC1 inhibitor) decreased the $[Cl^-]_i$, suggesting an NKCC1-dependent basolateral Cl^- uptake in ductal fragments and pancreatic organoids.

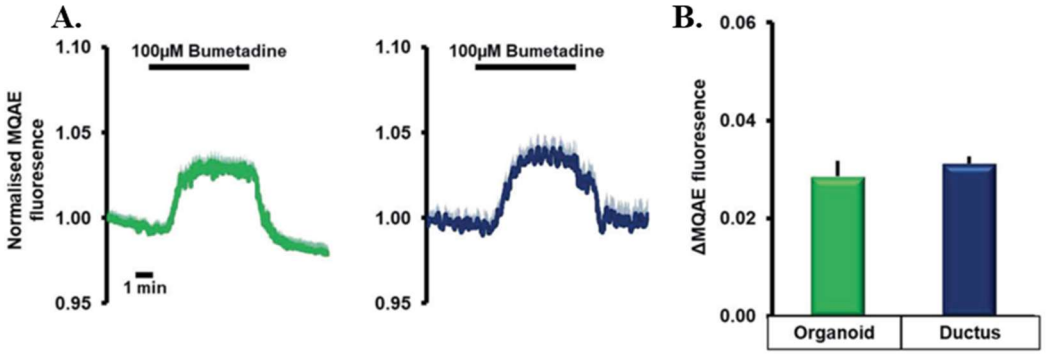

Figure 13. To measure NKCC1 activity, organoids and ductal fragments were treated with bumetanide in HCO_3^-/CO_2-buffered extracellular solution. Traces show the intracellular Cl^- level **(A)** and bar charts summarize the maximal fluorescent intensity changes **(B)** in pancreatic organoids (green) and ductal fragments (blue). Average number of experiments: n=4.

4.5. Comparison of basolateral HCO_3^- uptake in isolated ducts and pancreatic organoids

To compare the activity of basolateral Na^+-dependent HCO_3^- uptake in primary pancreatic ductal fragments and pancreatic OCs, we applied the above described NH_4Cl administration in Na^+-free HCO_3^-/CO_2-buffered solution. Under these conditions the recovery from acidosis was almost completely abolished confirming that this process strongly depends on the extracellular Na^+ and suggesting the potential role of NHE1 and NBCe1 in the process (Figure 14. A-B).

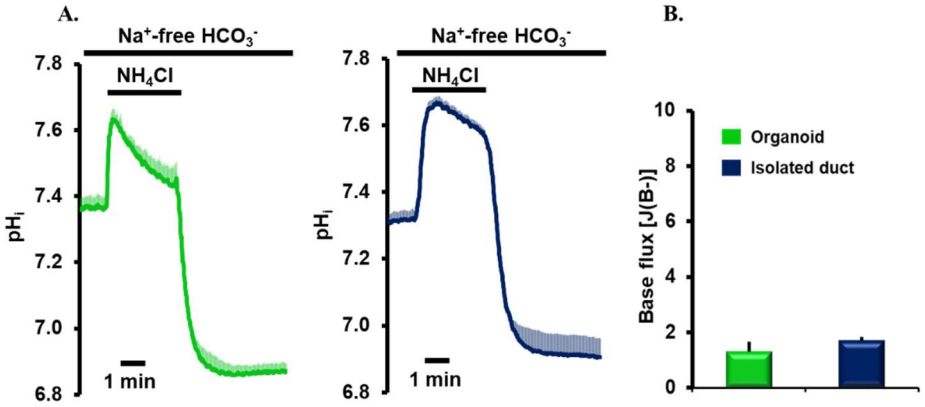

Figure 14. Bicarbonate secretion of pancreatic organoids and isolated ductal fragments in Na^+-free HCO_3^-/CO_2-buffered extracellular solution. **A.** Pancreatic organoids (green) or ducts (blue) were alkalized with 20mM NH_4Cl administration, the lack of recovery in Na^+-free solution highlights the role of Na^+ dependent transport processes in the recovery. **B.** Bar charts shows that basolateral Na^+ removal almost completely abolished the recovery from intracellular acidosis. Average number of experiments: n=4.

To characterize the contribution of each transporter in more details, we applied another protocol and specific inhibitors of NHE1 and NBCe1 (Figure 15.). During these series of experiments, the standard HEPES was switched to HCO_3^-/CO_2-buffered solution triggering a rapid drop in pH_i due to the influx and intracellular conversion of CO_2 to carbonic acid and its dissociation to HCO_3^- and H^+. In the presence of extracellular Na^+ the pH_i is restored to the resting level by NHE1 and NBCe1. As the average traces of individual experiments (Figure 15.) and the calculated base flux and $\Delta(pH_i)_{max}$ (Figure 16.) demonstrate, both primary ducts and pancreatic OCs showed similar responses to the specific inhibition of NHE1 (10 µM EIPA) and NBCe1 (10 µM S0859). In both cases the inhibition of NHE1 caused a higher decrease in the calculated base flux (79.01% in OC and 70.62% in ducts) compared to the inhibition of NBCe1 (60.82% in OC and 53.32% in ducts). The combined inhibition of NHE1 and NBCe1 did not decrease the basolateral Na^+ dependent HCO_3^- uptake further.

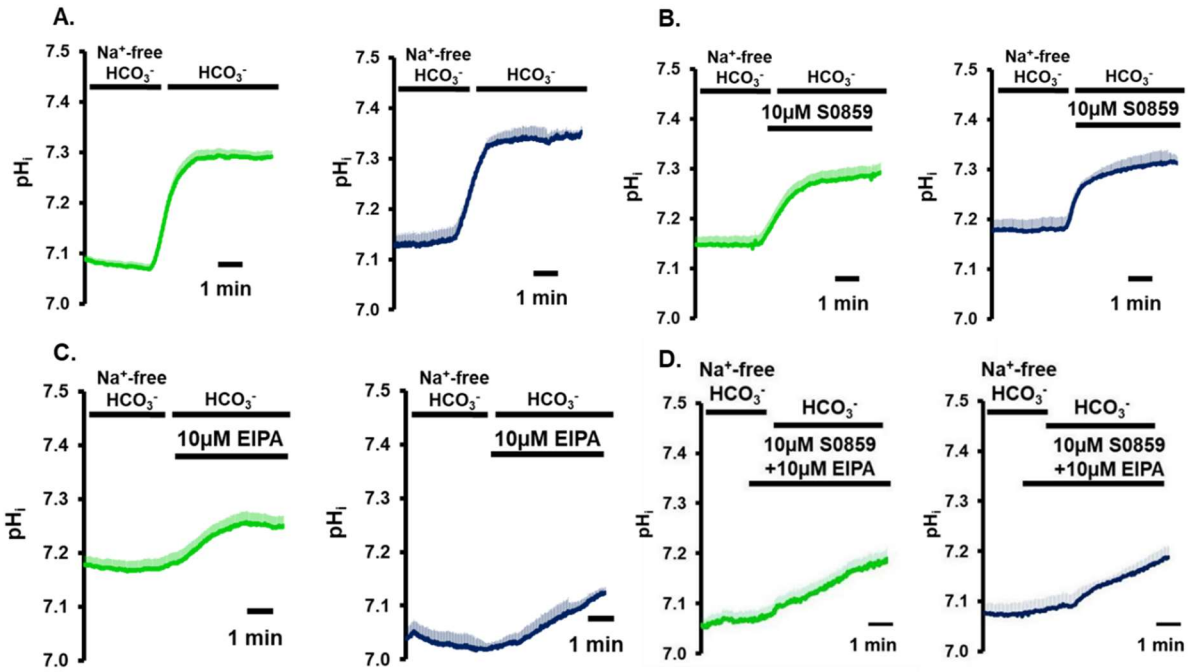

Figure 15. Mouse pancreatic organoids (green) and isolated ducts (blue) were perfused from the basolateral side with Na^+-free HCO_3^-/CO_2 buffered solution (**A**), followed 10μM S0859 in HCO_3^-/CO_2 buffered extracellular solution (**B**), followed by 10μM EIPA in HCO_3^-/CO_2 buffered extracellular solution (**C**), followed by the combination of inhibitors: 10μM S0859+10μM EIPA in HCO_3^-/CO_2 buffered extracellular solution (**D**). Average number of experiments: n=6.

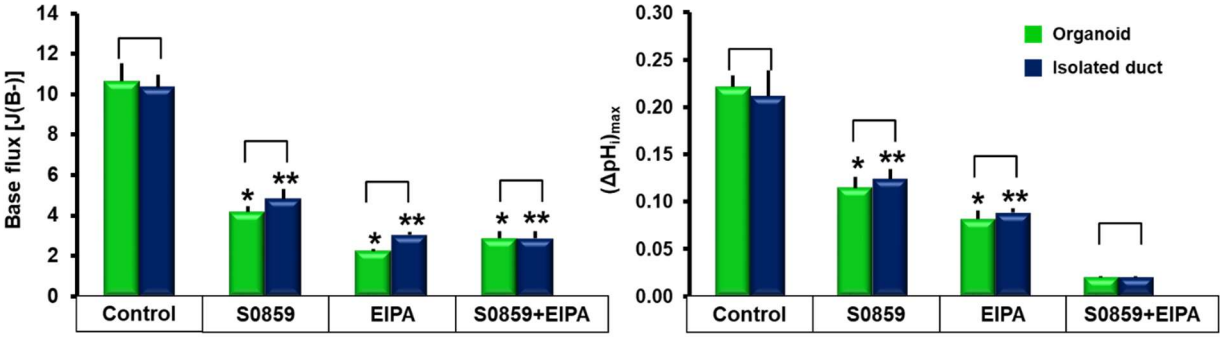

Figure 16. Bar charts summarize the effect of the inhibition. Acidic recovery and maximal pH_i changes decreased significantly by inhibition of NBCe1 (S0859) and/or NHE1 (EIPA). Representation of basolateral transport activities showed no difference in primary ducts and pancreatic organoids. Average number of experiments: n=4-6

4.6. Measurement of intraluminal pH in pancreatic organoids

HCO_3^- secretion of the pancreatic ductal epithelia determines the intraluminal pH of the pancreas, which has several crucial physiological roles, such as the neutralization of the H^+ ion

released by acinar cells during enzyme secretion (Gastroenterology. 2010 Nov;139(5):1711-20, 1720.e1-5.). Therefore, to follow changes of intraluminal pH real time we developed a novel fluorescent technique. In the first step we optimized the pH measurement with SNARF-1, which has commercially available dextran-conjugated version as well, suitable for extracellular pH measurements. OCs were loaded with SNARF-1 and challenged with 20mM NH_4Cl in standard HEPES, or HCO_3^-/CO_2 buffered solution (Figure 17. A-B), which resulted in similar pH_i changes as observed previously with BCECF. The recovery from alkali load was then then inhibited by $CFTR_{(inh)}$-172.

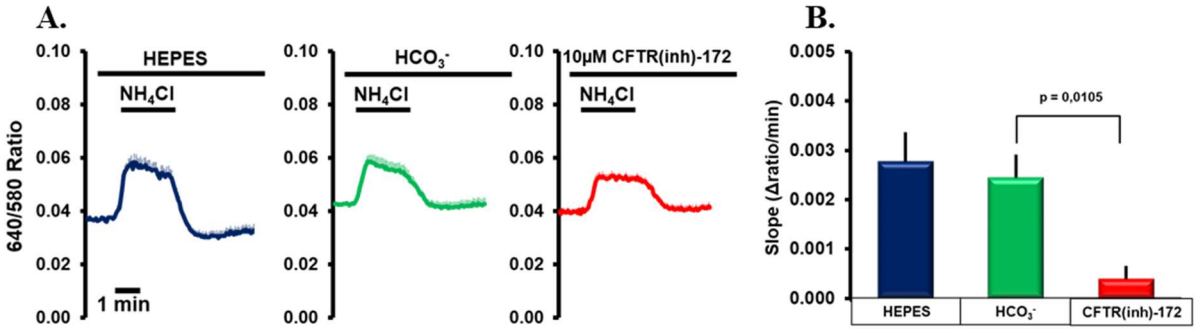

Figure 17. Intracellular pH (**A**) measurements of pancreatic organoids with SNARF-1 show similarity to the earlier results. Administration of 20mM NH_4Cl caused intracellular alkalosis followed by a slow regeneration in HEPES and HCO_3^-/CO_2 buffered solution, which was inhibited by $CFTR_{(inh)}$-172. **B.** Bar chart summarizes the effect of inhibition in intracellular measurements, which was calculated from curved slope of alkaline recovery. Average number of experiments: n=4-6.

Next, SNARF1-dextrane was injected into organoids using a micropipette, and the changes of intraluminal pH was recorded during the administration of NH_4Cl. As demonstrated on Figure 18. the injected dye stayed in the lumen and was not taken up by the epithelial cells.

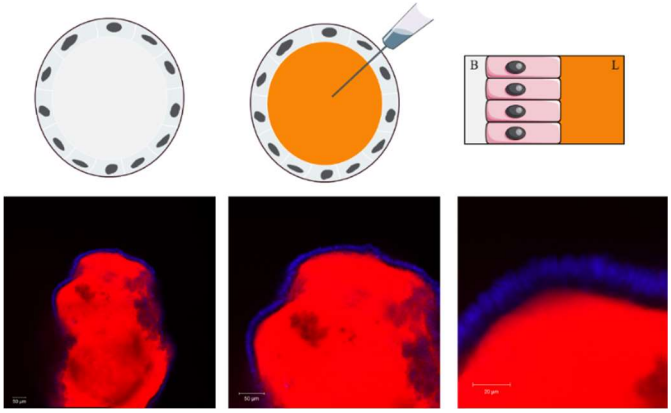

Figure 18. Schematic representation of the administration of SNARF1-dextrane to the lumen of the organoids and confocal images of the SNARF1-dextrane loaded organoids.

Administration of NH_4Cl in HEPES solution caused a moderate increase in the intraluminal pH which could be attributed to the diffusion of NH_3 into the organoid lumen (Figure 19). In contrast, NH_4Cl in HCO_3^-/CO_2-buffered solution triggered a rapid and notable elevation of intraluminal pH due to the efflux of HCO_3^- to the lumen. This elevation was completely abolished by 10µM $CFTR_{(inh)}$-172 administration suggesting the major role of CFTR in this process.

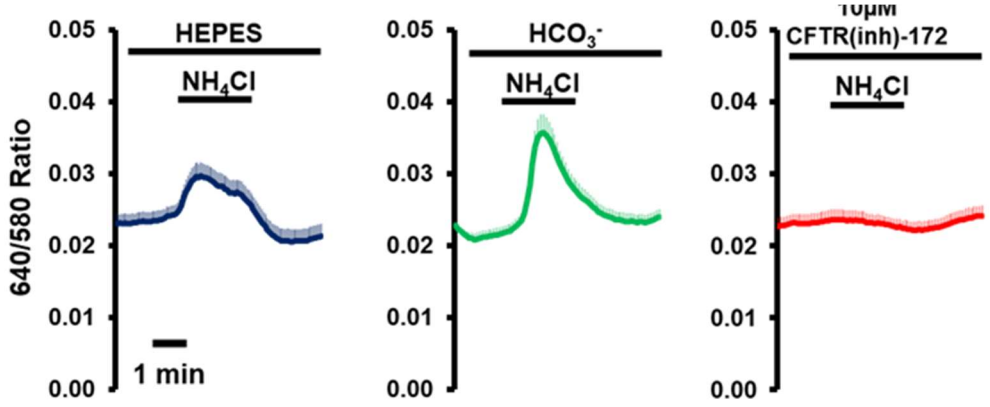

Figure 179. Intraluminal pH measurements of pancreatic organoids. Administration of 20mM NH_4Cl caused intraluminal alkalosis followed by a slow regeneration in HEPES and HCO_3^-/CO_2 buffered solution, which was inhibited by $CFTR_{(inh)}$-172. Notably, in the presence of HCO_3^- the increase was more rapid and the maximal increase was higher. Average number of experiments: n=4-6.

4.7. Morphological and functional polarity of pancreatic OCs

During our *in vitro* studies we observed remarkable similarities between the epithelial cells in isolated ductal fragments and OCs. Therefore, in the next step, we wanted to compare the morphology of the cells using scanning electron microscope (SEM). As demonstrated on Figure 20. the ductal cells show morphological polarity in both samples. In addition, epithelial cells in organoids form a polarized epithelial monolayer, whereas on the isolated ductal fragments several layers of connective tissue containing collagen fibers and fibroblasts can be observed.

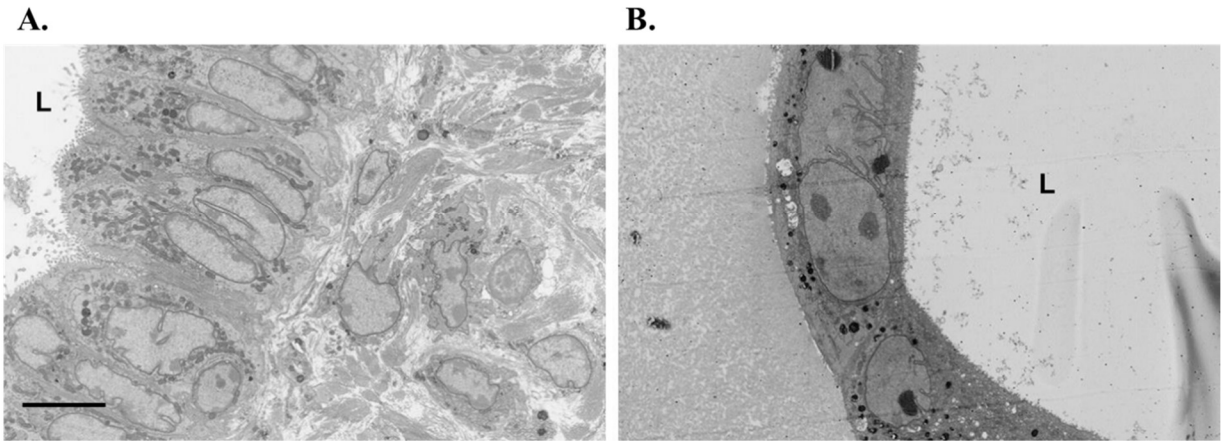

Figure 18. Representative SEM images of isolated ducts and OCs. **A.** Ultrastructure of pancreatic epithelium consists of multiple layers of adjacent fibroblasts masking the pancreatic ductal epithelial cells in isolated ducts. **B.** Ultrastructure of pancreatic epithelial organoids is consisted of a single epithelial monolayer. L: lumen; scale bars: 5 µm.

On the higher magnification SEM images (Figure 21.) the apical-basal polarity of primary ductal epithelial cells OC cells can be observed. On the apical membrane, we detected brush border in both samples (arrows), whereas mitochondria showed similar intracellular distribution around the lumen, forming a belt-like structure in the apical segment of the cells (arrowheads) both in OCs and isolated ducts.

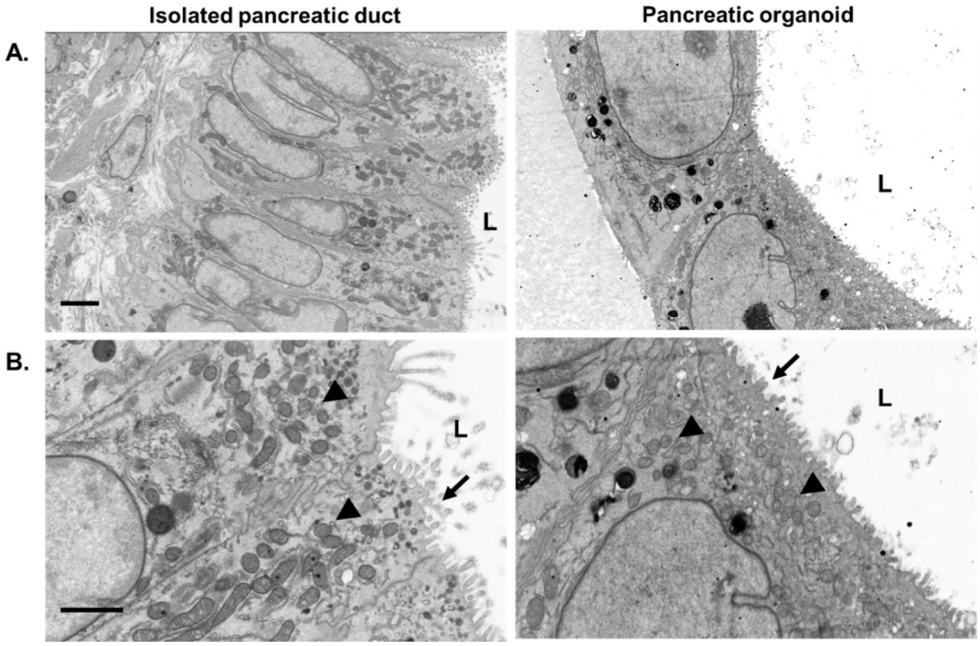

Figure 19. Representative scanning electron microscope images show the ultrastructure of epithelial cells in isolated ducts and in pancreatic organoids. Brush border was observed on the apical membrane in both samples (arrows), whereas most of the mitochondria were located in the apical region of the cells (arrowheads) both in organoids and in isolated ducts. L: lumen; scale bars: 2 µm in lower (**A**), 1 µm in higher magnification (**B**).

The functional measurements also suggested that besides the morphological polarity, the membrane proteins that determine ion secretion, show similar apical-basal polarity as well. To investigate functional polarity, immunofluorescent labeling of both the OCs and primary ducts was used. As demonstrated on Figure 22. the confocal images show that NHE1 and NBCe1 are expressed on the basolateral membrane, whereas CFTR is expressed solely on the apical membrane of the epithelial cells in both samples. These results confirmed the morphological and functional polarity of OCs.

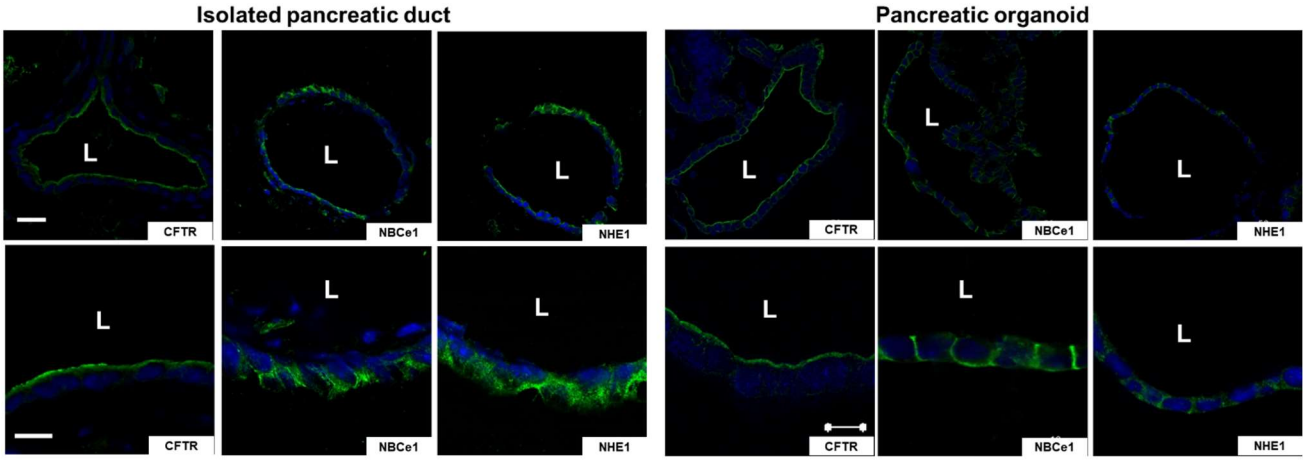

Figure 20. Immunofluorescent labeling. Representative confocal images demonstrate the polarized expression of proteins in both samples. NHE1 and NBCe1 are expressed on the basolateral, CFTR is expressed on the apical membrane. L: lumen; scale bars: 20 µm in upper panel, 10 µm in lower panel.

4.8. Use of pancreatic organoids in pathophysiological studies

As demonstrated above, pancreatic ductal OCs are suitable model to study ductal epithelial morphology and physiology. Another important area in the pancreatic research field is focusing on the pathophysiology of acute pancreatitis (AP). As detailed in the Introduction, our group previously provided evidence that pancreatic ductal cells play crucial role in the development of AP. As OCs could be utilized in pathophysiological studies as well, we wanted to compare pathophysiological Ca^{2+} signaling in response to chenodeoxycholate (CDC) – a non-conjugated bile acid known to trigger sustained intracellular Ca^{2+} elevation in ductal cells. As demonstrated on Figure 23. panel A and B, both OCs and isolated ductal fragments responded to CDC with sustained Ca^{2+} elevation. Notably, the elevation in OCs was higher, compared to ductal fragments, which might be explained by the lack of surrounding conjunctive tissue in case of

OCs, which may allow CDC to reach the epithelial cells in higher concentration. These results suggest that organoids can be used in pathological studies as well.

Our experiments in pancreatic acinar cells suggested that the redox-sensitive non-selective cation channel TRPM2 plays an important role in the pathogenesis of bile acid induced cell injury. To study this in ductal epithelial cells, first we compared the bile acid induced Ca^{2+} elevations in wild type and TRPM2 knockout ducts. By contrast, to acinar cells, no significant difference was detected in isolated ductal fragments between the Ca^{2+} response of WT and TRPM2 KO ducts to 250µM CDC, suggesting that, in ductal cells, TRPM2 plays no role in bile-acid-induced cell injury (Figure 23. B).

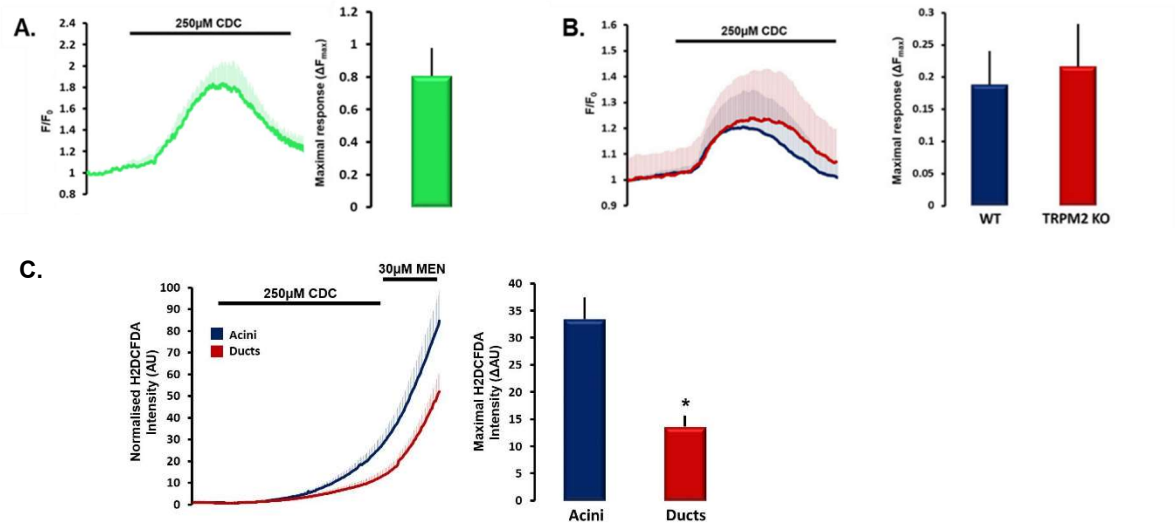

Figure 21. CDC induced Ca^{2+} signalization. Intracellular Ca^{2+} elevations evoked by 250µM CDC in WT and TRPM2 KO isolated ducts (**B**) and organoids (**A**). Average traces of H2DCFDA intensities and bar charts of the maximal fluorescent intensity changes in isolated acini and ducts (**C**). Average number of experiments: n=4-6. *: $p < 0.05$ vs acini.

To provide mechanistic explanation for the different contribution of TRPM2 in bile acid generated Ca^{2+} response in acinar and ductal cells, we measured the intracellular reactive oxygen species (ROS) using H2DCFDA. In accord with the previous findings of Booth et al. [53], we showed that 250µM CDC increased the intracellular ROS level in pancreatic acini. Interestingly, the ROS production during bile acid treatment in ductal epithelial cells was significantly lower compared to acinar cells (13.6±2 vs 33.4±4 arbitrary unit) (Figure 23. C). These results can explain our observation that TRPM2 knock-out ductal cells are not protected from bile acid induced sustained Ca^{2+} elevation. Based on these we didn't investigated this in further details in pancreatic OCs.

5. DISCUSSION

OCs have recently emerged as promising *ex vivo* models of tissue development, physiology and pathophysiology. Reports suggested that cells in OCs maintain tissue specific gene expression, cell morphology and function and may represent features of malignant diseases. Although organoids are used in an increasing number of studies, we only have limited experimental data about their physiological relevance, especially in case of pancreatic OCs. Therefore during my work we wanted to provide side-by-side comparison of gene expression, cell morphology and function of pancreatic ductal epithelial cells derived from primary isolated ductal fragments and of pancreatic OCs.

Ion (especially HCO_3^-) and fluid secretion is the primary function of the pancreatic ductal epithelia, which is obtained by the interaction of the electrogenic SLC26A6 Cl^-/HCO_3^- exchanger and the CFTR Cl^- channel [9, 10]. Due to the molecular interaction between the two proteins the ductal cells are able to secrete and maintain 140mM intraluminal HCO_3^- concentration (~5-6 fold higher than the intracellular) [54]. The current model suggests that in the proximal ducts CFTR provides the extracellular Cl^- for the Cl^-/HCO_3^- exchange of SLC26A6. However, in the distal pancreatic ducts, the anion exchange of SLC26A6 is not possible to maintain due to the very low luminal and intracellular Cl^- concentration. Under these conditions CFTR permeability is switched by With-No-Lysine (WNK)/STE20/SPS1-related proline/alanine-rich kinase (SPAK) kinases in favour of HCO_3^- [19]. On the opposite site, the accumulation of the HCO_3^- across the basolateral membrane is mediated by the electrogenic NBCe1. Another factor in this process is the passive diffusion of CO_2 through the membrane followed by the carbonic anhydrase-mediated conversion of CO_2 to HCO_3^- and H^+ [55]. In addition to these, NHE1 maintains the pH_i by transporting excess H^+ from the cells. Therefore, first we analyzed the expression of genes encoding these ion channels and transporters in isolated ducts and OCs. Our results confirmed the expression of these genes in primary mouse ductal fragments and also in pancreatic OCs. Moreover, the expression of *Atp12a* (encoding nongastric H^+/K^+ ATPase); *Kcnma1* (encoding BK channel), *Slc26a3* and *Nkcc1* overlapped in the two types of samples. We also found that four members of the voltage-gated potassium channel subfamily *Kcna1, Kcna2, Kcnd3* and *Kcnh1* are expressed in pancreatic epithelial cells, which have not been described earlier. In addition, we showed the expression of two voltage-gated Cl^- channels: *Clcn1* and *Clcn3* that were not suggested earlier. Transcription of *Clcn3* has only been described in pancreatic β-cells, where it is localized on insulin granules and play a role in insulin processing and secretion through regulation of granular acidification [56].

Moreover, our results showed that *Enac* and *Ano1* are expressed in both isolated primary ductal fragments as well as pancreatic OC. The relatively strong expression of *Enac* in pancreatic epithelia is somewhat unexpected since earlier studies were not able to demonstrate functional activity of ENaC in rat pancreatic ducts [57] and according to the current hypothesis ENaC is not expressed and has no role in exocrine pancreatic epithelial cells [9].

As mentioned earlier, only a limited number of studies have been published about the functional analysis of organoids. Recently Foulke-Abel *et al*. used human intestinal crypt-derived enteroids to investigate their functional relevance to ion transport physiology and pathophysiology [58]. Using undifferentiated and differentiated enteroids, they demonstrated that these organoids show similar apical-basal polarity to the human small intestine enterocytes and express functionally active NHE3, which is the most prominent transporter in this cell type. Organoid swelling was inhibited by inhibitors of CFTR, NKCC and NHE3. Whereas intracellular acidification caused by forskolin administration in HCO_3/CO_2^- buffered solution was created by CFTR and electrogenic NBC1. In 2018 O'Malley *et al.* reported the establishment of a culture system of differentiated pancreatic ductal epithelial cells in a polarized monolayer [59]. In this 2D air-liquid interface culture system, cells were grown on semipermeable filters and were reported to develop epithelial cell morphology. Short circuit current and extracellular pH measurements revealed that these cells respond to increase of intracellular cAMP and express functionally active CFTR channels. Although the culture system could overcome some limitations of isolated ductal fragments (such as the presence of contaminating fibroblasts) and it can be used for short circuit current measurements, it still possess the drawbacks of the 2D culture systems [60], whereas maintenance of this culture seems to be tedious and less efficient compared to 3D organoid cultures. Although functional data are limited, the described results highlighted that organoids might be a powerful *ex vivo* system to represent original tissue morphology and functions and could be used to model pancreatic ductal secretory functions in physiology and pathology. Therefore, in this study we performed functional analysis of pancreatic OCs and compared them with the well-studied isolated ductal fragments used as a reference point. Measurements of apical HCO_3^- secretion and basolateral HCO_3^- uptake were highly comparable in OCs and primary ducts. In addition, the activities of other ion transport processes mediated by NHE1, or NKCC1 were similar in the two systems. Finally, the Ca^{2+} signaling, which is one of the major signal transduction pathways in the pancreatic ductal epithelia [10], showed similar characteristics in OCs further supporting the functional equality of pancreatic organoids with the primary ductal system.

As mentioned in the introduction, the intraductal pH has a major importance in the exocrine pancreatic physiology. Earlier studies showed that protons are co-released during exocytosis of digestive enzymes thus causing significant intraluminal acidosis, which has to be compensated by ductal cells to avoid intrapancreatic trypsinogen activation [61] and the development of AP [62]. This was further confirmed in patients, where intraductal pH in acute biliary pancreatitis was significantly decreased compared to the controls (6.97 ± 0.13 vs 7.79 ± 0.20) [63]. Therefore, we developed a technique that utilizes dextran conjugated pH sensitive fluorescent dye SNARF1 to monitor pH changes in the lumen of the organoids. Using this technique, we were able to follow the pH elevation induced by NH_4Cl administration, which was completely blocked by CFTR inhibition.

Patient-derived pancreatic tumor organoids have been successfully used for disease modelling and to predict response to anticancer therapy [38, 64, 65]. In another study human pluripotent stem cells were used to generate acinar/ductal organoids to model cystic fibrosis [66]. In experimental setup that was more focused on organoid function Dekkers *et al.* used patient-derived rectal organoids to measure CFTR activity and predict response to CFTR corrector and/or potentiator therapy [67]. They used forskolin-induced swelling (FIS) which is currently the state-of-the-art technique to measure CFTR-dependent ion and fluid secretion [68]. Whereas FIS is relatively simple and robust method that correlates well with the individual response to cystic fibrosis treatment, it also might have some potential limitations. During forskolin stimulation the secreted fluid expands the lumen and the increasing intraluminal pressure prevents water efflux that might therefore not follow the ion current linearly. In addition, the increased tension might activate the mechanoreceptors (such as Piezo1) in the apical membrane of epithelial cells [69]. This shall not be a problem in samples with CFTR expression defects, where the initial fluid secretion is marginal [70]. However, in wild type pancreatic organoids FIS leads to a relatively rapid rupture of the organoids (data not shown). Therefore instead of measuring the relative luminal volume of the organoids, we utilized a $[Cl^-]_i$ sensitive fluorescent indicator to follow Cl^- movements in pancreatic OCs [71]. Our results with this technique are consistent with the literature data since forskolin significantly enhanced, whereas CFTR, or PKA inhibition markedly decreased the increase of fluorescent signal. Therefore, this technique could be potentially capitalized in pancreatic physiology research and in drug screening studies to identify compounds that improve exocrine pancreatic ductal secretion.

Finally, we compared the morphology of the isolated ducts and OCs with a special focus on apical-basal polarity. The ultrastructure of the epithelial cells in the two samples showed no

major difference and the OCs epithelial cells represented the same features – increased apical density of mitochondria, brush border on the apical membrane – like primary ductal cells. Importantly, the distribution of proteins showed similar pattern in cross sections of organoids and isolated ducts. We confirmed that CFTR is expressed exclusively on the apical, whereas NHE1 and NBCe1 were found on the basolateral membrane, which is concordant to the current literature [9, 72]. Taken together, our results demonstrated a complete overlap of gene expression and morphology of isolated ductal fragments and pancreatic OCs and more importantly the use of OCs can ensure that results are not derived from heterogeneous tissue fragments but from primary epithelial cell monolayers. Notably, these results also suggest that the exocrine pancreatic ductal secretion may be far more complicated than the currently used models suggest [7]. Further analysis will be needed to clarify the functional relevance of these results (especially the role of ENaC, CCls and K^+ channels) and special attention should be paid to species dependent alterations in expression and eventually in protein function. However, if protein expression and function confirms these findings, our results might indicate the need of revision of the current model of pancreatic ductal secretion.

As demonstrated above, pancreatic ductal OCs are suitable model to study ductal epithelial morphology and physiology. Another important area in the pancreatic research field is focusing on the pathophysiology of acute pancreatitis (AP). Previous reports suggest that bile acids can trigger sustained intracellular Ca^{2+} elevation, increase intracellular and intramitochondrial ROS production and damage the mitochondrial network in both pancreatic acinar and ductal cells. These subcellular changes can eventually lead to AP, which is a severe inflammatory disease of the gastrointestinal tract that has no specific treatment. Disturbed intracellular Ca^{2+} homeostasis has been suggested by several studies to play a pivotal role in bile-acid-induced exocrine pancreatic cell damage. In pancreatic acini, bile acids trigger dose-dependent intracellular Ca^{2+} elevation via the activation of IP_3 and ryanodine receptors [73]. In addition, Perides et al. showed that activation of the G-protein-coupled cell surface bile acid receptor (Gpbar1 or TGR5) at the apical membrane of pancreatic acinar cells leads to sustained Ca^{2+} elevation, intracellular activation of digestive enzymes and cell injury [74]. Moreover, the genetic deletion of Gpbar1 specifically reduced the severity of TLCS-induced AP. On the other hand, however, in pancreatic ductal cells, CDC dose-dependently elevated the intracellular Ca^{2+} level and inhibited HCO_3^- secretion [25]. To establish the pathophysiological utility of pancreatic OCs we compared pathophysiological Ca^{2+} signaling in response to CDC. Our results showed that both OCs and isolated ductal fragments responded to CDC with sustained

Ca^{2+} elevation. Notably, the elevation in OCs was higher, compared to ductal fragments, which might be explained by the lack of surrounding conjunctive tissue in case of OCs, which may allow CDC to reach the epithelial cells in higher concentration. These results suggest that organoids can be used in pathological studies as well. Our experiments in pancreatic acinar cells suggested that the redox-sensitive non-selective cation channel TRPM2 plays an important role in the pathogenesis of bile acid induced cell injury (not included to the thesis). In our experiments on pancreatic acinar cells, CDC increased the $[Ca^{2+}]_I$ both in acinar and ductal cells, but genetic deletion of TRPM2 decreased Ca^{2+} elevation only in acinar cells. The results of this study show that the TRPM2 channel has a ~22% contribution to the bile-acid-generated Ca^{2+} signal in acinar cells. To study this in ductal epithelial cells, first we compared the bile acid induced Ca^{2+} elevations in wild type and TRPM2 knockout ducts. By contrast, to acinar cells, no significant difference was detected in isolated ductal fragments between the Ca^{2+} response of WT and TRPM2 KO ducts to 250μM CDC, suggesting that, in ductal cells, TRPM2 plays no role in bile-acid-induced cell injury. Interestingly, our results highlighted that the generation of intracellular ROS in response to bile acids is remarkably different in pancreatic acinar and ductal cells, which can provide mechanistic explanation for the different involvement of TRPM2 in bile acid generated Ca^{2+} response in these cell types. This different response might be caused by the difference in the mitochondrial mass in acinar versus ductal cells [13, 75]. Based on these observations we did not investigate the role of TRPM2 in further details in pancreatic OCs.

Taken together, after thorough analysis, we have demonstrated that epithelial cells in OCs remarkably correspond with the primary ductal epithelia. Our results confirmed that pancreatic OCs could be a relevant, highly reproducible *ex vivo* model system with increased throughput to study pancreatic secretory physiology and pathology and thus could be a potential solution for an unmet need in pancreatic research.

6. SUMMARY

Background: The exocrine pancreas has an important role in the regulation of fluid and bicarbonate secretion. Studies of the physiology and pathophysiology of the exocrine pancreas are significantly limited especially in humans by the lack of reliable models with sufficient throughput. Recently developed pancreatic organoid culture (OCs) may help to overcome this barrier, however the morphology and physiology (such as ion secretory processes) in pancreatic OC are not completely known yet.

Aim: Our aim was to characterize the expression and regulation of ion channels and transport proteins in mouse pancreatic epithelial organoid cell cultures.

Method: In our experiments, pancreatic ductal fragments were isolated from FVB/N mice to generate three-dimensional organoid cultures and compare ion transport mechanisms to primary tissue. Mouse pancreatic ductal fragments were isolated by enzymatic digestion and cultured in Matrigel at 37°C for one week with special organoid media. Protein expressions were assessed by RT-PCR. Changes of the intracellular pH was measured with fluorescence microscopy using BCECF pH sensitive fluorophore to characterize the ion transporter activities of OCs and ductal fragments. Changes of intracellular Cl^- ion was measured with MQAE chloride sensitive dye to characterize apical Cl^- channel activity, especially the CFTR channel. Intraluminal pH was measured with confocal microscopy using SNARF1-dextrane. The morphology of primary tissue and OCs was investigated by immunofluorescent labeling and scanning electron microscopy. Changes of intracellular Ca^{2+} ion was measured with Fura-2-AM calcium sensitive dye to examine intracellular calcium release in TRPM2 KO and WT ducts.

Results: Gene expression analysis resulted overlapping patterns in OCs compared to freshly isolated ductal fragments. Basolateral administration of 20mM NH_4Cl led to rapid increase in intracellular pH in standard HEPES and HCO_3^-/CO_2 buffered solution. The administration of 10μM $CFTR_{(inh)}$-172, a selective inhibitor of CFTR decreased Cl^- ion secretion and the regeneration from the alkali load. Removal of NH_4Cl led to rapid intracellular pH reduction, which was followed by an extended recovery from acidosis. This recovery phase was fully inhibited by the lack of Na^+ ion, whereas specific NHE1 and NBCe1 inhibitors significantly decreased the HCO_3^- uptake. Measurements of intracellular pH and Cl^- level revealed no significant difference in the activities of the apical Cl^-/HCO_3^- exchange, or in the basolateral Na^+ dependent HCO_3^- uptake. In the intraluminal pH measurements 10μM $CFTR_{(inh)}$-172 resulted a decreased alkaline recovery in OCs. Morphological analysis of OCs revealed similar apical-basal polarity in OCs as in primary ductal epithelia. In pathophysiological studies, the administration of 250μM bile acid elevate the intracellular Ca^{2+} concentration in organoids, as

well as in TRPM2 KO and WT ductal fragments, nevertheless we could not observe significant difference.

Conclusion: Our study suggests that ion transport activities in mouse OC are similar to those observed in freshly isolated primary tissue. OCs are suitable model to study pancreatic ductal epithelial ion transport, and may help to highlight mechanisms and processes in health and diseases, that may increase the efficiency of drug development for secretory pancreatic disorders like cystic fibrosis, or chronic pancreatitis.

7. NOVEL RESULTS AND OBSERVATIONS

- Epithelial cells in pancreatic organoid cultures form monolayers with apical-basal polarity
- The ultrastructure of epithelial cells in organoid cultures in isolated ductal fragments display remarkable similarity
- Gene expression and distribution of ion channels and proteins overlap in organoid cultures in isolated ductal fragments
- The ion transport activities in mouse OC are similar to those observed in freshly isolated primary tissue
- The changes of the intraluminal pH can be followed in organoid cultures using SNARF-1-dextrane
- Bile acids trigger sustained Ca^{2+} elevation in OCs and in isolated ductal fragments

8. ACKNOWLEDGMENT

First of all, I would like to thank all the people who helped and supported me during my Ph.D studies. I would like to express my greatest appreciation and gratitude for my supervisor **Dr. József Maléth** and I would like to thank him for the many help he gave during my professional career. Present dissertation would not have been possible without his guidance. I owe my heartful gratitude to **Prof. Dr. Péter Hegyi** for giving me the opportunity to do my Ph.D studies in his prestigious research group.

I would like to gratefully thank **Prof. Dr. Csaba Lengyel**, the current-, and **Prof. Dr. György Ábrahám**, the former head of the First Department of Medicine University of Szeged, for giving me the opportunity to work in their institute.

In addition, I would like thank to **Prof. Dr. András Varró**, former-, and **Dr. István Baczkó**, current head of the Department of Pharmacology and Pharmacotherapy University of Szeged, that they permitted me to conduct my experiments in their institute.

I would like to express my appreciation to **Dr. Petra Pallagi** and **Prof. Dr. Zoltán Rakonczay** for their cooperation and scientific guidance, and I especially thank **Dr. Viktória Venglovecz** for her scientific help.

I wish to express my sincere thanks to all my colleagues and friends in the laboratory, in alphabetic sequence; **Kitti Ancsányi, Emese Réka Bálint, Dr. Eszter Becskeházi, Dr. Zsolt Balla, Dr. Péter Csernay-Bíró, Dr. Vivien Demeter-Haludka, Szilvia Déri, Klaudia Dobai, Attila Ébert, Gabriella Fűr, Eleonóra Gál, Zsuzsanna Gyömbér, Marietta Görög, Anna Grassalkovich, Xénia Katona, Evelyin Kelemen, Balázs Koncz, Dr. Eszter Kormányos, Anett Lőrincz, Tamara Madácsy, Brigitta Molnár, Dr. Gottfired Misklolczi, Margit Németh, Dr. Daniella Pigniczki, Dr. Andrea Szentesi, Dávid Tàlas, Dr. Emese Tóth, Árpád Varga.**

These acknowledgements would not be complete without mentioning my research lab assistants. I would like to express my appreciation for their help and skillful assistance; **Tünde Pritz, Miklósné Àrva, Rea Fritz, Zsolt Tóth, Nikoletta Szabó, Edit Magyarné Pálfi and †Erzsébet Zoltánné Fuksz.**

I acknowledge my gratitude to the **Theoretical Medicine Doctoral School** for permitting me to undergo my research.

I have to mention my sincere appreciation and honor to **Prof. Dr. Mihály Boros,** who convincingly conveyed a spirit of adventure in regard to research and encouraged me to enter the bloodstream of the scientific field. Because of this I would like express my respectable thank to **Dr. József Kaszaki, Dr. Tünde Tőkés, Dr. Petra Hartman, Dr. Eszter Tuboly, Dr. Gabriella Varga**, **Dr**. **András Tamás Mészáros and Dr. Szilárd Szűcs** for the many common scientific work and useful advices. Special thanks to all members of the Surgical Research Institute University of Szeged.

I would like to be one of the first to thank my partner, **Attila Ébert**, for his professional and general support, for showing me with his extensive knowledge and creativity that everything can be solved.

Finally, my deepest appreciation belongs to my family. I owe heartful thanks to my parents, **József Molnár** and **Éva Lak**, to my sisters **Brigitta Molnár** and **Dóra Molnár** and her husband **Dr. Bence Szalai** for all their patience, help and love, and that they believed in me and stood by me in all circumstances. They never stopped supporting me, therefore I dedicate this thesis to them.

Thank you for all my friends!

9. REFERENCES

1. Dahl-Jensen, S.B., et al., *Deconstructing the principles of ductal network formation in the pancreas.* PLoS biology, 2018. **16**(7): p. e2002842-e2002842.
2. Hegyi, P., et al., *The acinar-ductal tango in the pathogenesis of acute pancreatitis.* Gut, 2011. **60**(4): p. 544-552.
3. Venglovecz, V., et al., *Potassium channels in pancreatic duct epithelial cells: their role, function and pathophysiological relevance.* Pflügers Archiv - European Journal of Physiology, 2015. **467**(4): p. 625-640.
4. Stewart, A.K., et al., *Functional coupling of apical Cl-/HCO3- exchange with CFTR in stimulated HCO3- secretion by guinea pig interlobular pancreatic duct.* American journal of physiology. Gastrointestinal and liver physiology, 2009. **296**(6): p. G1307-G1317.
5. Argent, B.E., et al., *MORPHOLOGICAL, BIOCHEMICAL AND SECRETORY STUDIES ON RAT PANCREATIC DUCTS MAINTAINED IN TISSUE CULTURE.* Quarterly Journal of Experimental Physiology, 1986. **71**(4): p. 633-648.
6. Hegyi, P., M.A. Gray, and B.E. Argent, *Substance P inhibits bicarbonate secretion from guinea pig pancreatic ducts by modulating an anion exchanger.* American journal of physiology. Cell physiology, 2003. **285**(2): p. C268-C276.
7. Yamaguchi, M., et al., *Bicarbonate-rich fluid secretion predicted by a computational model of guinea-pig pancreatic duct epithelium.* J Physiol, 2017. **595**(6): p. 1947-1972.
8. Arkle, S., et al., *ISOLATION OF DUCTS FROM THE PANCREAS OF COPPER-DEFICIENT RATS.* Quarterly Journal of Experimental Physiology, 1986. **71**(2): p. 249-265.
9. Lee, M.G., et al., *Molecular mechanism of pancreatic and salivary gland fluid and HCO3 secretion.* Physiological reviews, 2012. **92**(1): p. 39-74.
10. Maleth, J. and P. Hegyi, *Calcium signaling in pancreatic ductal epithelial cells: an old friend and a nasty enemy.* Cell Calcium, 2014. **55**(6): p. 337-45.
11. Sewell, W.A. and J.A. Young, *Secretion of electrolytes by the pancreas of the anaestetized rat.* The Journal of physiology, 1975. **252**(2): p. 379-396.
12. Park, H.W. and M.G. Lee, *Transepithelial bicarbonate secretion: lessons from the pancreas.* Cold Spring Harbor perspectives in medicine, 2012. **2**(10): p. a009571.
13. Maléth, J., et al., *Non-conjugated chenodeoxycholate induces severe mitochondrial damage and inhibits bicarbonate transport in pancreatic duct cells.* Gut, 2011. **60**(1): p. 136.
14. Zhao, H., R.A. Star, and S. Muallem, *Membrane localization of H+ and HCO3- transporters in the rat pancreatic duct.* The Journal of general physiology, 1994. **104**(1): p. 57-85.
15. Donowitz, M., C. Ming Tse, and D. Fuster, *SLC9/NHE gene family, a plasma membrane and organellar family of Na^+/H^+ exchangers.* Molecular aspects of medicine, 2013. **34**(2-3): p. 236-251.
16. Xu, H., F.K. Ghishan, and P.R. Kiela, *SLC9 Gene Family: Function, Expression, and Regulation.* Comprehensive Physiology, 2018. **8**(2): p. 555-583.

17. Novak, I., et al., *Pancreatic bicarbonate secretion involves two proton pumps.* The Journal of biological chemistry, 2011. **286**(1): p. 280-289.

18. Gentzsch, M. and M.A. Mall, *Ion Channel Modulators in Cystic Fibrosis.* Chest, 2018. **154**(2): p. 383-393.

19. Park, H.W., et al., *Dynamic regulation of CFTR bicarbonate permeability by [Cl-]i and its role in pancreatic bicarbonate secretion.* Gastroenterology, 2010. **139**(2): p. 620-31.

20. Yang, D., et al., *IRBIT coordinates epithelial fluid and HCO3- secretion by stimulating the transporters pNBC1 and CFTR in the murine pancreatic duct.* J Clin Invest, 2009. **119**(1): p. 193-202.

21. Park, S., et al., *Irbit mediates synergy between ca(2+) and cAMP signaling pathways during epithelial transport in mice.* Gastroenterology, 2013. **145**(1): p. 232-241.

22. Hegyi, P. and Z. Rakonczay, *The role of pancreatic ducts in the pathogenesis of acute pancreatitis.* Pancreatology, 2015. **15**(4, Supplement): p. S13-S17.

23. Pallagi, P., et al., *The Role of Pancreatic Ductal Secretion in Protection Against Acute Pancreatitis in Mice*.* Read Online: Critical Care Medicine | Society of Critical Care Medicine, 2014. **42**(3).

24. Maléth, J., et al., *Alcohol disrupts levels and function of the cystic fibrosis transmembrane conductance regulator to promote development of pancreatitis.* Gastroenterology, 2015. **148**(2): p. 427-39.e16.

25. Venglovecz, V., et al., *Effects of bile acids on pancreatic ductal bicarbonate secretion in guinea pig.* Gut, 2008. **57**(8): p. 1102-12.

26. Kim, M.S., et al., *Native Store-operated Ca2+ Influx Requires the Channel Function of Orai1 and TRPC1.* The Journal of biological chemistry, 2009. **284**(15): p. 9733-9741.

27. Hong, J.H., et al., *Polarized but differential localization and recruitment of STIM1, Orai1 and TRPC channels in secretory cells.* Traffic (Copenhagen, Denmark), 2011. **12**(2): p. 232-245.

28. Pandol, S.J., et al., *Investigating the pathobiology of alcoholic pancreatitis.* Alcoholism, clinical and experimental research, 2011. **35**(5): p. 830-837.

29. Huang, W., et al., *Fatty acid ethyl ester synthase inhibition ameliorates ethanol-induced Ca2+-dependent mitochondrial dysfunction and acute pancreatitis.* Gut, 2014. **63**(8): p. 1313-1324.

30. Criddle, D.N., et al., *Ethanol toxicity in pancreatic acinar cells: mediation by nonoxidative fatty acid metabolites.* Proceedings of the National Academy of Sciences of the United States of America, 2004. **101**(29): p. 10738-10743.

31. Criddle, D.N., et al., *Fatty Acid Ethyl Esters Cause Pancreatic Calcium Toxicity via Inositol Trisphosphate Receptors and Loss of ATP Synthesis.* Gastroenterology, 2006. **130**(3): p. 781-793.

32. García, M., et al., *Pancreatic duct secretion: experimental methods, ion transport mechanisms and regulation.* Journal of Physiology and Biochemistry, 2008. **64**(3): p. 243-257.

33. Hollande, E., et al., *Expression of a wild-type CFTR maintains the integrity of the biosynthetic/secretory pathway in human cystic fibrosis pancreatic duct cells.* The

journal of histochemistry and cytochemistry : official journal of the Histochemistry Society, 2005. **53**(12): p. 1539-1552.

34. Fatehullah, A., S.H. Tan, and N. Barker, *Organoids as an in vitro model of human development and disease.* Nature Cell Biology, 2016. **18**(3): p. 246-254.

35. Dutta, D., I. Heo, and H. Clevers, *Disease Modeling in Stem Cell-Derived 3D Organoid Systems.* Trends in Molecular Medicine, 2017. **23**(5): p. 393-410.

36. Huch, M., et al., *Unlimited in vitro expansion of adult bi-potent pancreas progenitors through the Lgr5/R-spondin axis.* The EMBO journal, 2013. **32**(20): p. 2708-2721.

37. Simian, M. and M.J. Bissell, *Organoids: A historical perspective of thinking in three dimensions.* The Journal of cell biology, 2017. **216**(1): p. 31-40.

38. Boj, S.F., et al., *Organoid models of human and mouse ductal pancreatic cancer.* Cell, 2015. **160**(1-2): p. 324-38.

39. Kretzschmar, K. and H. Clevers, *Organoids: Modeling Development and the Stem Cell Niche in a Dish.* Dev Cell, 2016. **38**(6): p. 590-600.

40. Sato, T., et al., *Single Lgr5 stem cells build crypt-villus structures in vitro without a mesenchymal niche.* Nature, 2009. **459**(7244): p. 262-5.

41. Clevers, H., *Modeling Development and Disease with Organoids.* Cell, 2016. **165**(7): p. 1586-1597.

42. Takahashi, K. and S. Yamanaka, *Induction of Pluripotent Stem Cells from Mouse Embryonic and Adult Fibroblast Cultures by Defined Factors.* Cell, 2006. **126**(4): p. 663-676.

43. Hohwieler, M., et al., *Stem cell-derived organoids to model gastrointestinal facets of cystic fibrosis.* United European gastroenterology journal, 2017. **5**(5): p. 609-624.

44. Sato, T., et al., *Long-term Expansion of Epithelial Organoids From Human Colon, Adenoma, Adenocarcinoma, and Barrett's Epithelium.* Gastroenterology, 2011. **141**(5): p. 1762-1772.

45. Nusse, R. and H. Clevers, *Wnt/beta-Catenin Signaling, Disease, and Emerging Therapeutic Modalities.* Cell, 2017. **169**(6): p. 985-999.

46. Barker, N., et al., *Lgr5(+ve) stem cells drive self-renewal in the stomach and build long-lived gastric units in vitro.* Cell Stem Cell, 2010. **6**(1): p. 25-36.

47. MacDonald, B.T., K. Tamai, and X. He, *Wnt/beta-catenin signaling: components, mechanisms, and diseases.* Developmental cell, 2009. **17**(1): p. 9-26.

48. Novellasdemunt, L., P. Antas, and V.S.W. Li, *Targeting Wnt signaling in colorectal cancer. A Review in the Theme: Cell Signaling: Proteins, Pathways and Mechanisms.* American journal of physiology. Cell physiology, 2015. **309**(8): p. C511-C521.

49. de Lau, W., et al., *The R-spondin/Lgr5/Rnf43 module: regulator of Wnt signal strength.* Genes & development, 2014. **28**(4): p. 305-316.

50. Yamamoto, S., et al., *TRPM2-mediated Ca2+influx induces chemokine production in monocytes that aggravates inflammatory neutrophil infiltration.* Nat Med, 2008. **14**(7): p. 738-47.

51. Liu, X., et al., *Loss of TRPM2 function protects against irradiation-induced salivary gland dysfunction.* Nat Commun, 2013. **4**: p. 1515.

52. Gout, J., et al., *Isolation and culture of mouse primary pancreatic acinar cells.* Journal of visualized experiments : JoVE, 2013(78): p. 50514.

53. Booth, D.M., et al., *Reactive oxygen species induced by bile acid induce apoptosis and protect against necrosis in pancreatic acinar cells.* Gastroenterology, 2011. **140**(7): p. 2116-25.

54. Hong, J.H., et al., *Mechanism and synergism in epithelial fluid and electrolyte secretion.* Pflugers Arch, 2014. **466**(8): p. 1487-99.

55. Dyck, W.P., N.C. Hightower, and H.D. Janowitz, *Effect of acetazolamide on human pancreatic secretion.* Gastroenterology, 1972. **62**(4): p. 547-52.

56. Deriy, L.V., et al., *The granular chloride channel ClC-3 is permissive for insulin secretion.* Cell Metab, 2009. **10**(4): p. 316-23.

57. Novak, I. and M.R. Hansen, *Where have all the Na+ channels gone? In search of functional ENaC in exocrine pancreas.* Biochim Biophys Acta, 2002. **1566**(1-2): p. 162-8.

58. Foulke-Abel, J., et al., *Human Enteroids as a Model of Upper Small Intestinal Ion Transport Physiology and Pathophysiology.* Gastroenterology, 2016. **150**(3): p. 638-649 e8.

59. O'Malley, Y., et al., *Development of a polarized pancreatic ductular cell epithelium for physiological studies.* J Appl Physiol (1985), 2018. **125**(1): p. 97-106.

60. Horvath, P., et al., *Screening out irrelevant cell-based models of disease.* Nat Rev Drug Discov, 2016. **15**(11): p. 751-769.

61. Behrendorff, N., et al., *Protons released during pancreatic acinar cell secretion acidify the lumen and contribute to pancreatitis in mice.* Gastroenterology, 2010. **139**(5): p. 1711-20, 1720 e1-5.

62. Geisz, A. and M. Sahin-Toth, *A preclinical model of chronic pancreatitis driven by trypsinogen autoactivation.* Nat Commun, 2018. **9**(1): p. 5033.

63. Takacs, T., et al., *Intraductal acidosis in acute biliary pancreatitis.* Pancreatology, 2013. **13**(4): p. 333-5.

64. Huang, C. and C. Freter, *Lipid metabolism, apoptosis and cancer therapy.* International journal of molecular sciences, 2015. **16**(1): p. 924-949.

65. Tiriac, H., et al., *Organoid Profiling Identifies Common Responders to Chemotherapy in Pancreatic Cancer.* Cancer discovery, 2018. **8**(9): p. 1112-1129.

66. Hohwieler, M., et al., *Human pluripotent stem cell-derived acinar/ductal organoids generate human pancreas upon orthotopic transplantation and allow disease modelling.* Gut, 2017. **66**(3): p. 473-486.

67. Dekkers, J.F., et al., *A functional CFTR assay using primary cystic fibrosis intestinal organoids.* Nat Med, 2013. **19**(7): p. 939-45.

68. Dekkers, J.F., et al., *Characterizing responses to CFTR-modulating drugs using rectal organoids derived from subjects with cystic fibrosis.* Sci Transl Med, 2016. **8**(344): p. 344ra84.

69. Romac, J.M., et al., *Piezo1 is a mechanically activated ion channel and mediates pressure induced pancreatitis.* Nat Commun, 2018. **9**(1): p. 1715.

70. Boj, S.F., et al., *Forskolin-induced Swelling in Intestinal Organoids: An In Vitro Assay for Assessing Drug Response in Cystic Fibrosis Patients.* J Vis Exp, 2017(120).

71. Ko, S.B., et al., *A molecular mechanism for aberrant CFTR-dependent HCO(3)(-) transport in cystic fibrosis.* EMBO J, 2002. **21**(21): p. 5662-72.

72. Zeng, M., et al., *Restoration of CFTR Activity in Ducts Rescues Acinar Cell Function and Reduces Inflammation in Pancreatic and Salivary Glands of Mice.* Gastroenterology, 2017. **153**(4): p. 1148-1159.

73. Gerasimenko, J.V., et al., *Bile acids induce Ca2+ release from both the endoplasmic reticulum and acidic intracellular calcium stores through activation of inositol trisphosphate receptors and ryanodine receptors.* J Biol Chem, 2006. **281**(52): p. 40154-63.

74. Perides, G., et al., *Biliary acute pancreatitis in mice is mediated by the G-protein-coupled cell surface bile acid receptor Gpbar1.* Gastroenterology, 2010. **138**(2): p. 715-25.

75. Park, M.K., et al., *Perinuclear, perigranular and sub-plasmalemmal mitochondria have distinct functions in the regulation of cellular calcium transport.* EMBO J, 2001. **20**(8): p. 1863-74.